

A MODELING STUDY OF THE TROPICAL TROPOPAUSE LAYER

by

DANIEL HENZ

A thesis submitted in partial fulfillment of
the requirements for the degree of

Master of Science

(Atmospheric and Oceanic Sciences)

at the

UNIVERSITY OF WISCONSIN-MADISON

2010

ABSTRACT

The region in the tropical atmosphere between the level of main convective outflow (LMCO) and the cold point tropopause (CPT) or temperature minimum defines the tropical tropopause layer (TTL). Interaction between dominant convective processes in bulk troposphere and radiatively driven processes in the lower stratosphere result in the existence of the TTL. The TTL is significant in that it is decoupled from most explicit troposphere convective mixing, but is also not as isolated as the stratosphere. This “in between” is characterized by high concentrations of pollutants, relative humidity, and reduced visibility. The TTL is modeled in this study using a non-hydrostatic cloud resolving model in order to better understand how this layer is formed by these processes.

The model successfully simulates the TTL region without the need to remove the shear profile from the initialized sounding. The lapse rate minimum (LRM) is found at 10.5 km, the LMCO is located at ~13.5 km coincident with the vertical mixing barrier, the level of zero net radiation (LZRH) is found to be at 14.4 km at a potential temperature of 353.9 K, and the CPT is found at 16.5 km at a temperature of 200.8 K. Deep convection and mean large scale ascent moisten an initially dry TTL. Water vapor concentration in the TTL is approximately 3.5-7 ppmv and 1.2 ppmv at the CPT.

A series of experiments to test the sensitivity of the CPT and level of zero net radiation (LZRH) to varied ozone concentrations found that when the ozone concentration is increased by 15% or 30% over the entire profile this causes the cold point tropopause (CPT) to lower and warm (0.5 km and ~0.5 K), and when the ozone concentration is decreased by the same amounts this causes the CPT to raise and cool (0.5 km and ~0.5 K). An increase or

decrease of ozone above the vertical gradient in ozone (13.5 km) causes analogous results to the first two sets of experiments, while varying the ozone concentration below 13.5 km resulted in no appreciable changes to the CPT. All experiments cause the LZRH to raise between 100m-300m and the potential temperature to increase up to 3 K, contradictory to previous results from other studies suggesting that increases (decreases) in ozone would lower (raise) the height of the layer and decrease (increase) the potential temperature at the LZRH. These results suggest that there is a more complex interaction between convective and radiative processes determining the height and potential temperature of the LZRH.

TABLE OF CONTENTS

ABSTRACT.....	iii
ACKNOWLEDGEMENTS.....	vi
1 INTRODUCTION.....	1
1.1 Tropical tropopause layer.....	2
1.2 The Circulation of the upper troposphere lower stratosphere.....	9
1.3 Water vapor, deep convection, and dehydration	13
1.4 TTL cirrus.....	20
1.5 TTL ozone.....	23
1.6 Thesis outline.....	24
2 DATA.....	26
3 MODEL DESCRIPTION.....	28
3.1 Experiment design.....	28
4 CONTROL EXPERIEMENT.....	35
4.1 Radiative-Convective Equilibrium.....	35
4.2 Control Run Results.....	37
4.3 Summary.....	48
5 SENSITIVITY EXPERIMENT.....	52
5.1 Sensitivity to ozone.....	52
5.2 Summary.....	59
6 CONCLUSIONS.....	62
REFERENCES.....	67

ACKNOWLEDGEMENTS

Thanks to my advisor, Greg Tripoli, for his patience, encouragement, advice and assistance with the UW-NMS; my committee members Matt Hitchman and Pao Wang for their invaluable insight and thoughts. Special thanks goes out to Tempei Hashino for all of his help with FORTRAN and adjustments made to the UW-NMS. I would also like to thank my family for their love and support and to Rachel, in particular, for always being there to listen. To the many fellow graduate students who made graduate school enjoyable, your friendship and support will always be remembered. A final thanks goes out to the entire faculty in the AOS department who have helped shape my meteorological understanding over the past several years.

APPROVED

Advisor Title:

Gregory J. Tripoli, Ph.D.

University of Wisconsin – Madison

Department of Atmospheric and Oceanic Sciences

Advisor Signature

Date

CHAPTER 1

INTRODUCTION

Radiative, convective, and chemical coupling between the tropical troposphere and stratosphere are among the many important processes that must be understood in order to accurately predict change in the tropics. Over the last two decades significant attention in the science community has been paid to studying the tropical upper troposphere and lower stratosphere as various processes in this region are known to strongly modulate global climate change. In recent years, the advent of higher resolution global climate models (GCMs) capable of simulating coupled air-sea interactions with the use of parameterizations have opened the door to these types of studies, but are severely limited by the accuracy of assumptions made in the various parameterizations. The sub-grid scale processes occurring in these model domains can be better understood through the use of cloud resolving models (CRMs) which can explicitly simulate these processes.

The primary focus of this thesis is to conduct a modeling study of the tropical tropopause layer to determine the role of physical processes occurring in this region without the need to parameterize the effects of deep convection. For this purpose a non-hydrostatic CRM coupled with observational data profiles is employed. The goal of modeling is threefold: 1) to fulfill the experiment design to successfully simulate the formation and maintenance of the tropical tropopause layer from an initial dry tropical sounding including shear, 2) to replicate the types of observations seen during field programs and previous research, and 3) to examine the sensitivity of this layer to various important species and physical processes that are modeled within the region.

1.1 Tropical Tropopause layer

The transition region between the tropical troposphere and the stratosphere has come to be known as the Tropical Tropopause Layer (TTL, also referred to as Tropical Transition Layer). The notion of the tropopause as a sharp boundary that separates the troposphere and stratosphere characterized by an abrupt change in lapse rate (that adheres to certain criterion) as is commonly defined, is not considered a complete definition in tropical latitudes. It has been widely accepted for some years (e.g. Highwood and Hoskins, 1998; Holton and Gettelman, 2001) that the TTL shares characteristics of both the upper troposphere and lower stratosphere (UTLS), and therefore is better defined as a layer rather than a boundary. The TTL is believed to be maintained by the interaction of convective transport, convectively generated waves, radiation, cloud microphysics and the large scale stratospheric circulation (Gettelman et al., 2009). In order to form a complete understanding of the TTL, a general vertical description of the tropical atmosphere and dominant processes involved will be presented (from previous research and literature) from the tropical troposphere, through the TTL region and into the lower stratosphere. Next, a synthesis figure combining all crucial levels and processes will be presented to examine the current state of the science. Finally, the remainder of this section will seek to group the three general definitions of the vertical and lateral bounds of the TTL.

The tropical troposphere, to a first order approximation, can be thought of as being in a state of near radiative-convective equilibrium (RCE) in which mean net radiative cooling through much of the troposphere, as is seen in a pure tropical radiative equilibrium profile, is compensated by the release of latent heat from moist convection (convective adjustment). This is the basis for early work done by Manabe and Strickler (1964), Manabe and Wetherald

(1967), and a central theme behind RCE models. Given that much of the tropical troposphere is under the influence of negative (sinking) vertical motion, tropical deep convection mainly remains confined to the Inter tropical Convergence Zone (ITCZ) associated with the upward and rising branch of the thermally direct Hadley Circulation and zonally overturning Walker Circulation.

Transitioning into the middle/upper tropical troposphere and near the base of the TTL, the influence of convection begins to weaken with height above the Level of Main Convective Outflow (LMCO) around 14 km (Alcala and Dessler, 2002), which agreeably coincides with the level of main poleward flow in the Hadley Circulation around 250-150 hPa (Peixoto and Oort, 1992). Studying ozonesondes above Samoa during the Pacific Exploratory Mission (PEM), Folkins et al. (1999) found strong correlation between a minimum in lapse rate in the temperature profile and a minimum in concentration in the ozone profile around 12 km. Above this layer they noticed a sharp vertical gradient in ozone, subsequent inhibition of tropical deep convection above 14 km, and termed this region as the ‘vertical mixing barrier’. Using extensive radiosonde and ozonsonde data, Gettelman and Forster (2002) found that the level of the lapse rate minimum (LRM), typically around 10-12km, represented the maximum in convective impact on upper tropospheric temperatures and closely corresponded to a minimum in ozone (O₃ min) just above this level. Their work was in agreement with previous studies done by Folkins et al. (1999), namely that most deep convection in tropics did not cross the vertical mixing barrier and tailed off at the LMCO. Alternatively, other work that had been conducted by Sherwood and Dessler (2001) made the assumption using parcel theory that while most convection tails off around the LMCO the effects of convective turrets overshooting their level of neutral buoyancy (LNB) were not

being taken into account (detailed discussion in Section 1.3.1). Acting under this assumption, Dessler (2002) found that significant detrainment of overshooting convection over the western Pacific was occurring as high as ~ 380 K potential temperature (~ 17 km), with as much as 60% of the mass crossing the 380 K surface detraining above 370 K (~ 15 km). This contrasted previously published suggestion that convective transport of mass does not significantly influence the composition of the atmosphere above 14 km. Using a satellite-borne precipitation radar on board the Tropical Rainfall Measuring Mission (TRMM) satellite, Alcala and Dessler (2002) found that $\sim 5\%$ of total deep convection contains overshooting into the TTL near the tropopause supporting the work done by Dessler (2001).

Above the mixing barrier and outside of overshooting convection the tropical atmosphere often remains in clear sky conditions, where radiation balance determines the direction and magnitude of vertical motion. Radiative heating in the TTL is a result of heating from the absorption of infrared radiation by ozone and carbon dioxide balanced by infrared cooling mostly from water vapor (Thuburn and Craig, 2002). In this region a transition occurs where the background clear sky radiative heating rate changes from a net cooling to a net heating (Sherwood, 2000; Folkins et al., 2000). This is termed the level of zero net radiative heating (LZRH) or $Q=0$. In clear sky conditions, this level is situated around 15 km or 360 K potential temperature (Gettelman et al., 2004). Corti et al (2005) found that in full (cloudy) sky conditions this transition occurs about 0.5-1.0 km lower than in clear sky. The existence of this level has led to the general assumption that in order to reach stratosphere, convection has to transport air at least to 360 K, from where radiative heating continues to lift the air to the cold point tropopause in large scale upwelling (Corti et al., 2006).

Transitioning to the UTLS or the region above the LZRH including the traditional lapse rate tropopause, the cold point tropopause (CPT) and level of highest convective overshooting (LHCO), lies at the base of the stratospheric Brewer-Dobson circulation and in the heart of the TTL. Tropical tropopause layer cirrus (TTLC) and subvisible cirrus (SVC) clouds are also located in this region, and have become the focal point for TTL research over the last half decade due to their radiative properties and impact in this region (discussed in detail, Section 1.4). The traditional barrier between the troposphere and stratosphere is the lapse rate tropopause. The World Meteorological Organization defines it as the lowest level at which the lapse rate decreases to $2^{\circ}\text{C}/\text{km}$ or less, provided that the average lapse rate between this level and all higher levels within 2 km does not exceed $2^{\circ}\text{C}/\text{km}$. It has already been pointed out that in the tropics this definition is not complete, and early work by Reid and Gage (1985) point out that this level is rather arbitrarily defined for operational use and has limited physical relevance. The CPT or temperature minimum is located typically around ~ 17 km or 380 K potential temperature. This level was deemed important for stratospheric-tropospheric exchange (STE) by Selkirk (1993). He found different types of convection raised or lowered the potential temperature and associated intense STE only with occasions on which it was lowered. Various authors (e.g. Holton and Gettelman, 2001) note the importance of the CPT because of its potential role in setting the stratospheric entry humidity due to its proximity to the level of minimum saturation vapor mixing ratio. Above the CPT lies the stratospheric inversion associated with radiational heating from ozone production/destruction. Convection has been known to penetrate into and above this region (17-19 km) on rare occasions (e.g. Adler and Mack, 1986; Danielsen, 1993; Liu and Zipser, 2005). For this reason a final important level, the level of highest convective overshooting

(LHCO) typically around 18.5 km or 70 hPa (Corti et al., 2006; Jensen et al., 2009; Fueglistaler et al., 2009), has been added in recent literature marking the top of the TTL.

1.1.1 Defining the TTL

Defining the TTL as a layer instead of at a fixed location opens the door to multiple definitions as to its vertical extent. It is clear in the literature that various definitions exist mainly on the vertical boundaries of the TTL. Resulting discrepancies on the placement of these boundaries by differing authors is a direct result as to what the author deems as most central to qualitative and/or theoretical understanding of the topic. It is important to emphasize here that more than one definition is clearly needed at this point in order to fully understand all the various processes involved. Figure 1 (below) provides a general depiction of the TTL emphasizing the layers and dominant processes within the region as described earlier. The three general definitions of the vertical bounds of the TTL that are bracketed on the right side of the figure are meant to help explain differing schools of thought and the evolution of the definition of the TTL over the last decade.

The first definition denoted by 'A' (Fig. 1) sets the lower bound at the LMCO around 10-14 km and in particular around the LRM and O3 Min. The upper bound is placed at the CPT or temperature minimum around 17 km (Folkins, 1999; Gettelman and Forster, 2002; Thuburn and Craig, 2002; Gettelman et al., 2004; Kuang and Bretherton, 2004). Acting under the assumptions that most convection is heavily influenced by the LRM and sharp gradient in ozone just above and that significant convection does not overshoot or penetrate above the LMCO except on rare occasions, these authors all form a similar definition for the lower bound of the TTL. These authors also share the same idea that the CPT is the upper bound of the TTL.

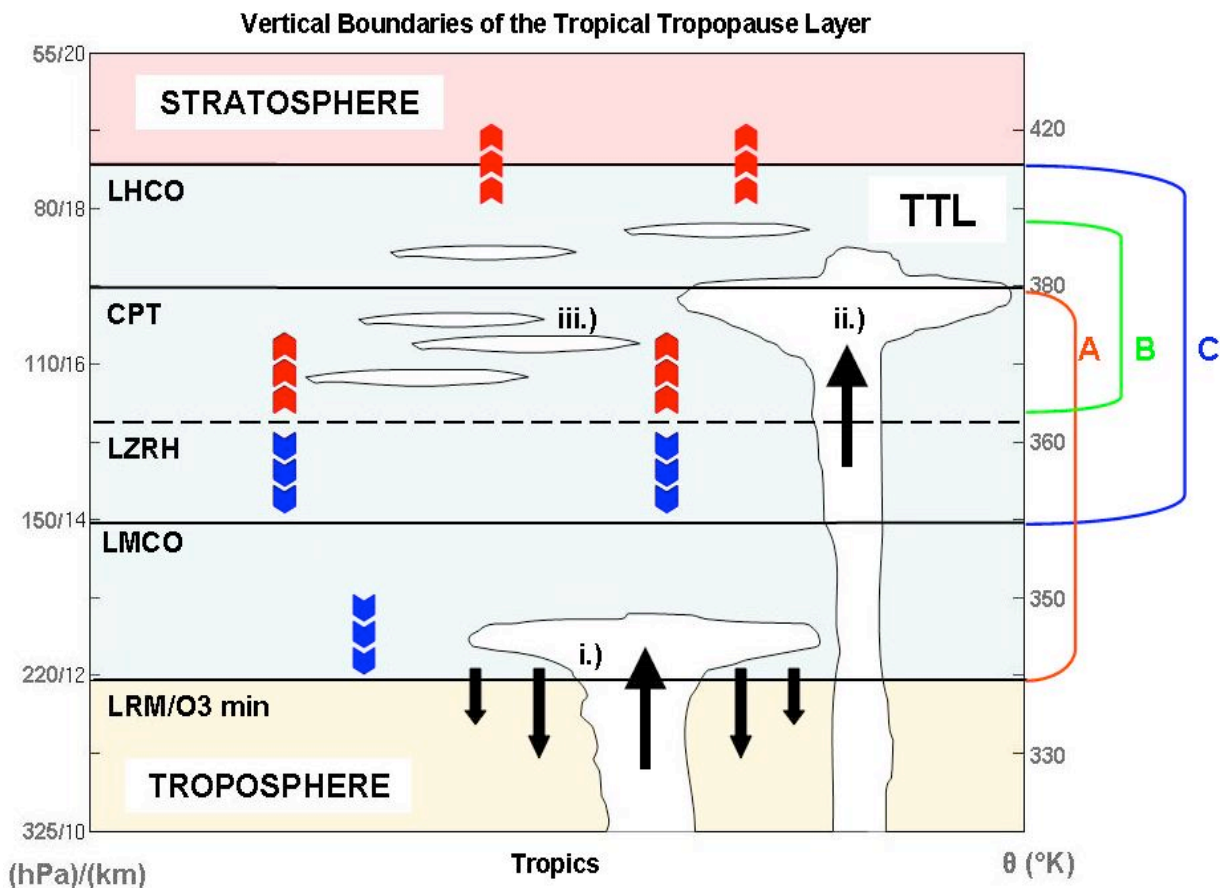


Figure 1: Schematic of critical levels and dominant processes within the TTL. i.) Typical convection, main outflow around 200 hPa. ii.) Rare overshooting deep convection, penetrating tropopause. iii.) Ubiquitous tropical tropopause cirrus and sub-visible cirrus. Black up arrows inside convection represent upward vertical motion in convective towers. Thin black down arrows represent downward vertical motion (subsidence). Blue dashed arrows represent radiative cooling (sinking motion). Red dashed arrows represent radiative heating (rising motion). LRM/O3 min: lapse rate minimum and ozone minimum. LMCO: level of main convective outflow. LZRH: level of zero net radiative heating, $Q=0$. CPT: cold point tropopause. LHCO: level of highest convective outflow. The colored letters A, B, and C on the right bracket the top and bottom boundaries of the TTL from previous literature and studies (discussed in detail in 1.1.1). Note: The height-pressure-potential temperature relations shown on the vertical axis are based on tropical annual mean temperature fields and previous studies. Horizontal axis is supposed to represent a region within the lateral bounds of the TTL from $\sim 30^{\circ}\text{N}$ - 30°S latitude (Subtropical Jets).

The second definition denoted by 'B' (Fig. 1) sets the lower bound of the TTL at the LZRH around 15 km, while the top is located somewhere between the CPT and LHCO around 17-19 km (Sherwood and Dessler, 2000, 2001; Dessler, 2002; Fueglistaler and Fu, 2006; Fu et al., 2007; Immler et al., 2008).

These authors share similar views that deep convection will overshoot its LNB and that occasionally it can penetrate directly into the lower stratosphere above the CPT. They see convection as playing an important role in conjunction with the radiation balance associated with the LZRH as to which air can preferentially enter the lower stratosphere.

The third definition denoted by 'C' (Fig. 1) places the bottom boundary at around 14 km or the LMCO and the top boundary is denoted by the LHCO around 18-19 km (Corti et al., 2006; Fueglistaler et al., 2009; Jensen et al., 2009). This is more of a synthesis definition incorporating all the previous research on this topic. It is very similar to definition 'B' in determining the lower bounds. These authors challenge the top boundary as the CPT presented in definition 'A' by placing the top bounds to the LHCO where rare overshooting deep convection has been known to penetrate. Fueglistaler et al. (2009) argued that the CPT in many ways exhibited a maximum in TTL characteristics and therefore should be apart of the TTL instead of the upper bound.

The lateral bounds of the TTL are not typically discussed in detail in the literature. The lack of a formal definition as to the latitudinal extent of the TTL seems implausible given the amount of attention in the literature and lack of consensus apparent in its vertical boundaries. However, recently Fueglistaler et al. (2009) proposed that latitudes lower than 30° encompass the lateral reaches of the TTL or more specifically the region equatorward of the subtropical jets, by recalling earlier work from Haynes and Shuckburgh (2000). They

found that meridional transport in the lower TTL is limited by the large gradients in potential vorticity associated with the subtropical jets. Understanding the horizontal transport associated with the stratospheric Brewer Dobson circulation and tropospheric Hadley circulation (discussed in the following section, 1.2) seems to be the key to understanding the meridional extent of the of the TTL.

1.2 The circulation of the upper troposphere lower stratosphere

In terms of large scale processes, the tropical atmosphere is largely dominated in the troposphere by thermally direct Hadley circulation in the troposphere and large scale upwelling associated with the Brewer-Dobson circulation in the Stratosphere. The fact that the transition between these processes is smooth has led reasoning to the existence of the TTL (Corti et al., 2006). This section will seek to provide an overview of the dominant processes occurring in the troposphere and stratosphere that intertwine in the TTL region, and this author will refer the readers to the selected references as needed for a more in depth analysis of each individual process.

1.2.1 Tropospheric Circulation

The thermally direct Hadley circulation consists of rising motion in the tropics (ITCZ region), meridional flow towards the poles in the upper troposphere, sinking motion in the subtropics (outside of 30 North and South latitudes), and return flow near the surface towards the equator (Held and Hou, 1980; and references within). The rising branch of the circulation migrates north and south with the seasons and is normally found in the summer hemisphere, but due to complex ocean dynamics does not follow the latitudinal extent of maximum solar heating (e.g. the rising branch remains a few degrees North of the equator in the eastern

Pacific during southern Hemisphere Summer. The zonal counter part of the aforementioned Hadley Circulation is the Walker Circulation most prominent along the equatorial belt in the Pacific Ocean. This rising branch is generally found over the western Pacific, eastward flow is observed in the upper troposphere, sinking motion occurs in the western Pacific and westward return flow occurs near the equator (e.g. Bjerknes, 1969; and references within). The Walker circulation can slow or even reverse causing enhanced convection to extend eastward into the Pacific as this circulation is closely tied with ocean dynamics and the El Niño Southern Oscillation (ENSO). These circulations are similar in that generally regions under the influence of the rising (sinking) branches experience enhanced convection (low precipitation) and increased (decreased) relative humidity throughout the tropopause.

The third tropospheric circulation pattern in the tropics that is relevant to the TTL is the upper tropospheric subtropical highs associated with the Asian and North American monsoons. The basic drive for the monsoon circulation is provided by the contrast in thermal properties of the land sea surfaces, which leads to a continental and seasonal scale sea breeze circulation. As a result a pressure gradient force is developed at upper levels directed from land to ocean and the divergent wind that develops as a result to this pressure gradient causes a net mass transport out of the air column above the continent thereby creating a surface low over the continent (e.g. Holton, 1992). Enhanced convergent winds develop at low levels increasing boundary layer equivalent potential temperatures making the environment more favorable for deep convection. The south Asian and North American monsoons are deep circulations, with closed anticyclones extending up to at least 70 hPa in the stratosphere (Gettelman et al., 2004; and references within). They found using a chemical tracer model that the Asian monsoon circulation may contribute up to 75% of the total net upward water

vapor flux in the tropics at tropopause levels and some of this air may enter the tropical stratosphere bypassing the tropical tropopause altogether.

On intraseasonal time scales, conditions in the TTL are affected by the eastward-propagating Madden Julian Oscillation (MJO). In the convection portion of the MJO, convection moistens and warms the upper troposphere up to around 200 hPa, but cools and dries the layer 150-100 hPa (Fueglistaler et al., 2009). Interannual variability arises from changes in the distribution of convection associated with ENSO (Gettelman et al., 2001). During El Niño phases, the temperature pattern in the upper troposphere attenuates, and temperatures are fairly uniform. Thus, STE and dehydration in the TTL are more zonally uniform (Fueglistaler and Haynes, 2005).

Lateral mixing between the tropical upper troposphere and extratropical lower stratosphere is limited in the region of the subtropical jets with strong gradients in potential vorticity (e.g. Haynes and Shuckburgh, 2000). Two kinds of processes contribute to this exchange: 1.) advection southward and then westward around the southeast side of the monsoon anticyclones, and 2.) lateral Rossby-wave breaking in adjacent oceanic regions, such as over the mid Pacific (Fueglistaler et al., 2009).

1.2.2 Stratospheric Circulation

Brewer (1949) and Dobson (1956) were the first to describe the general features necessary to explain stratospheric measurements of water vapor and ozone. Studying meridional and seasonal distribution of stratospheric tracers, they deduced that air preferentially rises from the tropical troposphere into the stratosphere. Since the Brewer-Dobson circulation draws air through the TTL, processes in this region exert important controls over stratospheric humidity, which affects stratospheric radiation, chemistry, and

potentially the tropospheric climate as well (Kley et al., 2000). Since their early work, the existence of mean ascent in the tropical stratosphere is now well established (e.g. Rosenlof, 1995; Mote et al., 1998; Plumb and Eluszkiewicz, 1999). The basic structure of the Brewer-Dobson circulation consists of a single mean meridional cell in each hemisphere with rising motion in the tropics, poleward flow at midlatitudes, and downward cross-tropopause flow at high latitudes. Its effects can be felt all the way down to 125 hPa (Fueglistaler, 2009) in the middle of the TTL. For an in-depth explanation of the theoretical underpinnings of this circulation see Holton et al., (1995). The Brewer-Dobson circulation is also the basis for the ‘atmospheric tape recorder’ signal (Mote et al., 1996) as it accounts for the seasonal variation of tropopause temperatures and transport into the lower stratosphere (discussed in section 1.3).

Much interest has been paid into determining what drives the Brewer-Dobson circulation (meridional stratospheric circulation). Early work by Dunkerton (1978) deduced that air parcels in the extratropical stratosphere and mesosphere are driven poleward through angular momentum surfaces by a zonal torque, arising from the dissipation of eddies such as Rossby waves and gravity waves. Thus, mass continuity requires that the poleward flow is compensated by upward flow in the tropical lower stratosphere. Holton et al. (1995) also emphasized the role of waves and eddies in the extratropical stratosphere. They discussed how wave induced forces drive an extratropical ‘fluid dynamical suction pump’ and that this global scale circulation drives the stratosphere away from radiative equilibrium. This general concept of the stratosphere governing the behavior of in large regions of troposphere below has come to be known as ‘downward’ control (Highwood and Hoskins, 1998). Plumb and Eluszkiewicz (1999) challenged the assumptions behind downward control and the

extratropical pump stating that wave driving alone can not explain the fact that upwelling occurs in the tropics. Using a 2-d model they generated a steady and linear circulation with qualitative upwelling in the tropics. They emphasized that wave driving by wave drag was the dominant mechanism to explain tropical upwelling and that diabatic heating played a smaller but important role.

It has been shown (e.g. Rosenlof, 1995) that the meridional stratospheric circulation has an annual cycle, with larger net upward mass flux in the tropics during northern hemisphere winter than during summer. The annual cycle in upward tropical mass flux follows the annual cycle in downward mass flux in the northern hemisphere extratropics. They also argue that the annual zonal momentum forcing in northern hemisphere stratosphere is controlling mass flux in the lower stratosphere both in the tropics and northern hemisphere extratropics. Semi annual variations of wind and temperature exist in the mid and upper stratosphere. The quasi-biennial oscillation (QBO) dominates the variability of the equatorial stratosphere (~16-50 km) and is easily seen as downward propagating easterly and westerly wind regimes, with a variable period averaging approximately 28 months (Baldwin et al., 2001). The QBO can induce variability of temperature in the TTL on the order of 1 K at the tropopause.

1.3 Water vapor, deep convection, and dehydration

Water vapor is one of the key tracers for STE that led Brewer (1949) to deduce that air enters the stratosphere primarily across the tropical tropopause. Despite very small concentrations in the UTLS (~3-5 ppmv), water vapor is the most important contributor to the radiation balance in the TTL (Gettelman et al., 2004). The phase changes of water, from vapor to liquid or ice, are so strongly controlled by temperature that in the tropics the average

concentration of water vapor drops by four orders of magnitude from the surface to the tropical tropopause (Fueglistaler et al., 2009). That being said, reliable measurements of water vapor at the low concentrations that are found in the TTL are quite difficult to come by. Observational data from in situ measurements are limited to special campaigns which are restricted spatially and temporally. Another major problem of water vapor observations is that relatively large biases between instruments used to measure concentrations remain unresolved (Kley et al., 2000).

Up to about 150 hPa, the spatial and temporal patterns of water vapor concentrations largely follow that of deep convection (e.g. Zhu et al., 2000), with higher concentrations in convectively influenced regions. In the TTL, minima in water vapor concentrations are found generally in regions of low temperature anomalies such as above the Western Pacific warm pool (Fueglistaler et al., 2009). Important early studies of the TTL water vapor budget note that profiles of water vapor in the tropical lower stratosphere have a vertical structure and time dependence that are determined, to a first order approximation, by the ascent of the seasonally varying tropopause-level water vapor mixing ratio (Mote et al., 1996). The tropical lower Stratosphere thus resembles a “tape recorder” in that the water vapor content of rising air is marked by the seasonally varying saturation mixing ratio that it encountered at the tropical tropopause (Mote et al., 1998). Thus, water vapor can be used as a tracer to determine the origin of the air entering the lower stratosphere and also how that air effects stratospheric chemical and radiative processes. The air’s preferential entering the lower stratosphere in the tropics (Section, 1.2) and processes that control the water vapor minimum (dehydration, discussed in Section 1.3.2) seen in the upper TTL are the main reasons and motivation for much of the research in the TTL.

1.3.1 Deep Convection

Convection plays an important role in determining the thermodynamic properties and chemical composition of the TTL. The altitude at which convection detrains is constrained by the equivalent potential temperature (θ_e) or the potential temperature when all latent heat is released of air parcels within the tropical boundary layer, CAPE, and by the degree to which convective updrafts are affected by entrainment. This concept was studied by Selkirk (1987) during the Stratosphere-Troposphere Exchange Project/Australian Monsoons Experiment (STEP/AMEX) in 1987. In the absence of mixing, convection will detrain at its LNB, which is approximately equal to the height at which its equivalent potential temperature becomes equal to the potential temperature of the background atmosphere. Folkins et al. (2002) found a threshold of $\theta_e \geq 345$ K at which air parcels first attain positive CAPE, and may participate in convection. Studying cold point potential temperature and boundary layer potential temperature at Koror (7°N/134°E) with data from the Tropical Ocean Global Atmospheres/Coupled Ocean Atmosphere Response Experiment (TOGA/CORE) in 1992, Fueglistaler et al. (2009) found most of the air parcels below 900 hPa exceeded a θ_e of 345 K, the distribution of the θ_e peaks around 350 K and some parcels have θ_e larger than 370 K. This showed that in principle that some convection could reach the stratosphere locally by detrainment at the LNB. They also noted that a substantial fraction of air parcels has θ_e exceeding the potential temperature of the LZRH (~ 355K-360 K) meaning air parcels detrained at this height would incur tropical upwelling and continue to rise potentially to the stratosphere.

Air parcels can rise above the LNB by overshooting. Simply put, a parcel lifted in an unstable atmosphere will reach its LNB with a non-zero velocity, having been exposed to an upward buoyancy force below the LNB. The level of maximum overshoot refers to the maximum altitude that an air parcel would attain if all the buoyancy work done on the air parcel below the LNB is converted to kinetic energy at the LNB, and this kinetic energy is then used to do work against the downward buoyancy force above the LNB. Overshooting air parcels become progressively colder with height than the environment. If they mix with ambient air of higher potential temperature, they will cool these levels and eventually reach equilibrium at an altitude above their initial LNB (Fueglistaler et al., 2009).

The convective mass flux above the LMCO significantly decreases with height. There is ample evidence (e.g. Danielson, 1993; Dessler, 2002; Liu and Zipser, 2005; Fu et al., 2007) of convective detrainment into the lower parts of the TTL and even occasionally above the CPT. Because of increasing residence times in the TTL this convective mass flux likely plays an important role in determining chemical and physical properties. However, large uncertainties in the convective detrainment rate profile remain, and more work on developing a quantitative understanding of the impact of convection is needed (Fueglistaler et al., 2009).

1.3.2 Dehydration

As was stated earlier, much of the research that has focused on the study of the TTL was driven by the need to gain a better understanding of how and why air enters the stratosphere (Sections 1.1 and 1.2). Secondly, it is important to understand what processes control the water vapor minimum ‘hygropause’ seen in the tropical UTLS. Brewer (1949) explained the aridity of the stratosphere by arguing that nearly all air parcels entering stratosphere must cross the tropopause in the tropics where they are freeze dried to the

saturation characteristics of the CPT. While Brewer's qualitative model is generally accepted, there has been much debate on the physical, dynamical, and radiative processes involved.

Some early studies (e.g. Danielson, 1993; Sherwood and Dessler, 2001) suggest that dehydration is controlled by convective scale motions. Here convection overshooting creates anomalously cold air parcels with very low ice saturation mixing ratios. This is followed by detrainment and subsequent mixing of cloud air with stratospheric air. However, Holton and Gettelman (2001) state that efficient dehydration requires that an air parcel remain at or near the temperature of the tropical tropopause for sufficiently long so that ice crystals formed by the freeze drying process can sediment out, and it is not clear whether or not convective overshooting can meet that requirement. Studies in favor of this (Highwood and Hoskins, 1998; Folkins et al. 1999; Gettelman et al., 2001) suggest that overshooting of tropical convection into the interior of the TTL is not a common occurrence. More recent studies using CRMs yield contradictory results. Kuang and Bretherton (2004) found evidence for convective overshoot to induce drying. Jensen et al. (2007) found that convection tends to hydrate the TTL unless it is initially supersaturated. Grosvenor et al. (2007) found that results from 3-d CRMs yield a moistening effect, whereas 2-d models that can not resolve a realistic wind shear yield a drying effect due to lack of mixing of the overshoot with ambient air. Using remote sensing measurements of ice crystals during convection penetrating into the lower stratosphere Corti et al. (2008), found these convective events had a hydrating effect on the lower stratosphere due to evaporation of the ice particles and found no signs of convectively induced dehydration in the stratosphere.

The other perspective on dehydration suggests that large scale slow vertical ascent dominates mass transport across the tropical tropopause and that slow ascent is required for

effective dehydration. Newell and Gould-Stewart (1981) first argued that the ice saturation mixing ratio at the mean temperature of the tropical tropopause is too high to account for the observed stratospheric mixing ratios if cross-tropopause motions occur uniformly through the tropics. This idea gave rise to their 'stratospheric fountain' hypothesis where transport of air into the stratosphere occurs preferentially in areas where tropical tropopause temperatures are below their annual and longitudinal mean values. The coldest tropopause temperatures are found in the western Pacific in Northern Hemisphere winter. Thus, this region came to be known as the 'fountain' region. While several studies (e.g. Highwood and Hoskins, 1998) point out that, Newell and Gould-Stewart's analysis was hampered by the use of 100 hPa temperatures rather than CPTs. Studies using observational data and model results (e.g. Sherwood, 2000; Gettelman et al., 2001) found that the tropical western Pacific is actually an area with net subsidence at the tropopause and subvisible cirrus clouds are commonly observed.

Holton and Gettelman (2001) addressed this paradox that the tropical western Pacific has the exceptionally cold tropopause temperatures necessary for freeze drying due to upwelling, yet is under net subsidence. They changed the name of this region from stratospheric fountain to the 'cold trap'. Holton and Gettelman (2001) point out that it may be horizontal rather than vertical motion that ensures that a large fraction of air entering the stratosphere is exposed to the exceptionally low temperatures observed over the tropical western Pacific/Maritime continent area. Hartmann et al (2001) also suggested that horizontal advection of air could explain the cold trap hypothesis. They showed that air parcels that crossed the tropopause upstream of the cold trap could provide the moisture source for maintenance of the thin cirrus near the tropopause. At the same time particle sedimentation

out of the cirrus would dehydrate air to mixing ratios less than the saturation mixing ratio at the tropopause outside of the cold trap region. This result was in agreement with the hypothesis posed earlier by Jensen et al. (1996a) that gradual lifting near the tropopause accompanied by the formation of cirrus could account for necessary dehydration.

To this date no consensus exists within the research community as to an exact mechanism for dehydration of air into the lower stratosphere exists. Rather it is believed to be a combination of large scale upwelling and modification by deep convection. However, Holton and Gettelman's cold trap hypothesis and subsequent studies gave rise to studying the physical, dynamical, radiative, and chemical effects of thin cirrus formed in the TTL. It is now widely accepted that cirrus formed from deep convection, in situ, gravity waves, or Kelvin waves play a crucial role for air entering the stratosphere through the TTL. Thus, the next section will be devoted to explaining cirrus within the TTL.

1.4 TTL Cirrus

Recently, a significant amount of research of the tropical UTLS has shifted to studying the occurrence of ubiquitous cirrus clouds located in the TTL. It has come to be known that TTL cirrus may have a significant impact on the radiation budget due to absorption of outgoing longwave radiation (OLR) and emission at the very low tropical tropopause temperature (Jensen et al., 1996a). TTL cirrus may also be the most important mechanism in regulating water vapor entering the stratosphere, as they could serve as the missing link between tropospheric deep convection and the stratospheric Brewer-Dobson circulation (e.g. Corti et al., 2006). Given the large role these clouds play, the physical, dynamical, radiative, and chemical effects of thin cirrus formed in the TTL have been studied significantly over the past two decades.

1.4.1 TTL cirrus occurrence

For the last several decades it has been known that extensive cirrus decks are frequently found in the high altitudes of the tropics and more specifically located within TTL. For example, (Wang et al., 1996) noted that optically thin cirrus were present in the upper most tropical troposphere over the western Pacific during northern hemisphere winter about 50-80% of the time. McFarquhar et al. (2000) found that cirrus located within the TTL were present 29% of the time during the Central Equatorial Pacific Ocean Experiment (CEPEX). Pfister et al. (2001) noted during aircraft flights over the central Pacific during the Tropical Ozone Transport Experiment/Vortex Ozone Transport Experiment (TOTE/VOTE) during boreal winter of 1995/1996 that thin cirrus were detected above the aircraft 65% of the time. The altitudes of these clouds exceeded 18 km at times. They also divided cirrus observations into two basic types: thin quasi-laminar wisps and thicker more textured structures. More recently Dessler et al. (2006) used the Geoscience Laser Altimeter (GLAS) to access the frequency of thin cirrus during a 6 week period of northern hemisphere autumn 2003. Their study found a maximum frequency of occurrence of 28% over the West Pacific warm pool on the 360K potential temperature surface. The frequency of TTC was found to decrease with increasing altitude, but with little change in the spatial variability.

1.4.2 TTL cirrus classification and formation

TTL cirrus are defined as cirrus with an optical depth less than approximately 1, and they may be further subclassified as sub-visual cirrus (SVC) for an optical depths less than 0.03 (Sassen and Cho 1992). McFarquhar et al. (2000) found that based on the threshold of 0.03, the majority of thin cirrus are sub-visual. Most cirrus forming at cold temperatures are optically thin because there is little water vapor available to condense at such cold

temperatures. Measurement from various studies (e.g. Jensen et al., 1996b; Winker and Trepte, 1998; Pfister et al., 2001; Lawson et al., 2008) find these cirrus to be anywhere from several hundred meters to several kilometers thick and with significant horizontal extent ranging up to 2700 km across (Winker and Trepte, 1998; Lawson et al., 2008).

There are two generally accepted and heavily studied mechanisms for the generation of TTL cirrus: 1.) anvil blow off associated with tropical deep convection, 2.) in situ nucleation of ice crystals due to turbulent mixing from synoptic scale uplift (Jensen et al., 1996b). Massie et al. (2002) found that formation of TTL cirrus via anvil blow off was supported by the co-location of cirrus to convection. Luo and Rossow (2004) using trajectory analysis found that the decay of deep convection is immediately followed by the growth of cirrostratus and cirrus, and then the decay of cirrostratus is followed by the continued growth of cirrus. Fierli et al. (2008) using observations from the 2004 HIBISCUS campaign and results from a mesoscale model and trajectory analysis, found that cirrus clouds had formed in the outflow of a large persistent convective regions. Massie et al. (2002) noted that most of the cirrus clouds near the tropopause are located outside of regions of deep convection.

While convective outflow generates a net source of ice crystals, it does not provide a good explanation as to why SVC will tend to persist near the tropopause for long time periods of time. The persistence of TTL cirrus is determined by their microphysics (Jensen et al., 2009). Convective blow-off may be comprised of relatively large ice crystals as they have had plenty of time to grow in a moisture rich environment, whereas in-situ nucleation most often will produce very small ice crystals. These small ice crystals will have slow fall velocities allowing clouds to persist in the ice supersaturated region for long time periods. Thus, while the anvil blow-off mechanism is supported by the co-location of cirrus and

convection, microphysical arguments would better support in-situ nucleation. In situ formation of TTL cirrus requires a cool temperature anomaly (e.g. Kelvin wave or gravity wave) and regions of ice supersaturation, which together would tend produce ice crystals by homogeneous nucleation (Jensen et al., 1996b).

Immler et al. (2008) using radiosonde data and ECMWF analysis, link the occurrence of thin cirrus with temperature anomalies caused by equatorial Kelvin waves and in particular thin ice clouds formed regularly where cold anomalies shifted the tropopause to high altitudes. Other studies (e.g. Pfister et al. 2001; Garrett et al., 2004 and 2006) link gravity waves shed from deep convection to in situ formation of cirrus due to the temperature anomalies seen in their cold (rising) and warm (sinking) phases of propagation.

1.4.3 TTL cirrus microphysics

Given the vertical proximity of the location of TTL cirrus (14-19 km) and difficulties that arise in trying to gather much needed in situ observational data of ice crystals inside TTL cirrus, extensive field campaigns remain the best way for gathering this data. For example measurements of SVC over Kwajalein, Marshal Islands, by the WB-57F aircraft equipped with cloud probes found concentrations of small (less than 10 μm) particles are an order of magnitude greater than concentrations of larger size crystals (McFarquhar et al. 2000). The high concentrations of very small ice crystals with very slow fall speeds means TTL cirrus can exist for extended periods of time. However, recent studies have document the existence of significantly larger ice crystals. During the Costa Rica Aura Validation Experiment (CR-AVE) in 2006, Lawson et al. (2008) found large ice particles within TTL cirrus on order of 100 μm .

Observations from field experiments such as the ones above are necessary in order to aid in the modeling of TTL cirrus. Numerous modeling studies have been conducted in order to understand cirrus microphysical properties such as ice formation from convective anvils (e.g. Jensen et al., 1996b; Garrett et al., 2004 and 2006;), homogenous ice crystal formation (e.g. Jensen et al., 1996b; Jensen et al., 2009;), heterogeneous ice crystal formation (e.g. Jensen et al., 2007; Jensen et al., 2009), radiative properties of cirrus ice crystals (e.g. Corti et al., 2006; Fueglistaler and Fu, 2006; Durran et al., 2009) and more recently the direct role of aerosols (e.g. Kazil et al., 2007; Froyd et al., 2010).

1.4.4 Linkage to troposphere-stratosphere transport

The radiative heating of thin TTL cirrus has been estimated as sufficient to produce temperature increases of at least 2-3 K per day (Jensen et al. 1996b; McFarquhar et al. 2000) and could potentially exert a significant influence on the radiative balance of the TTL. Wang et al. (1996) estimated these sub-visual clouds contribute as much as 1 W/m^2 of OLR cooling, with a net positive forcing of up to $+1 \text{ W/m}^2$ in the tropics. This heating has been widely appreciated as having the potential to both warm and dissipate the cloud or to induce upward motion (Jensen et al., 1996b; Durran et al., 2009). If heating does induce a persistent ascent of the cirrus layer, these clouds may play an important role in the transport of water vapor into the tropical stratosphere (Jensen et al., 1996a; Corti et al., 2006). Corti et al. (2006) goes so far as to say that cloud lofting by cirrus represents missing second stage of TST, where the first stage is deep convection and final stage is the Brewer-Dobson circulation.

1.5 TTL ozone

Ozone is far more abundant in the stratosphere than in the troposphere, and hence is a tracer frequently used in the studies of STE and for studies in the TTL (e.g. Folkins et al., 1999; Xie et al., 2008). In the lower troposphere ozone is photochemically produced in regions of highly polluted surface air and biomass burning. Net ozone destruction occurs in the tropical boundary layer and in particular over the oceans (Jacob et al., 1996). Studies (e.g. Folkins et al., 1999) have linked low ozone concentrations in the tropical boundary layer with the O_3 min typically found around 12 km. They also discussed the impact of the sharp vertical gradient in ozone around 14 km (vertical mixing barrier) and its effects on the inhibition of convection above this level. Above the vertical mixing barrier and into the stratosphere ozone concentrations increase strongly with height as it is photochemically produced and is a net source in tropical stratosphere. It has been shown that the largest impact of ozone changes on climate occurs near the tropopause (Xie et al., 2008) or within the TTL. Using a GCM they found that a 15% increase of ozone in the TTL region is comparable to a 15% increase in the total ozone profile, a net warming effect ~ 2 K in the stratosphere, and a decrease of the tropical tropopause as a result to more water vapor entering the stratosphere.

1.6 Thesis Outline

Chapter 2 presents the host of observational and model data used for the simulations in this study. Updated ozone and carbon dioxide profiles gathered from observational data are presented. A prescribed background vertical motion profile meant to replicate lifting associated with the ITCZ region and the background initial sounding used to initiate convection in the domain are also presented in this chapter.

Chapter 3 describes the UW-NMS model that is employed for running all the simulations in this study. This chapter also discusses in detail the experiment design implemented, in particular: determining the height of the Rayleigh friction layer, dealing with trapped two dimensional gravity waves as a result to the inclusion of vertical shear with initial sounding, and implementing background vertical motion, ozone, and carbon dioxide profiles.

Chapter 4 discusses in detail the results from the control run. The model is run to RCE and the critical levels located within the TTL are located and described. The final section of this chapter discusses implications for the sensitivity study to follow.

Chapter 5 presents the results of the sensitivity study conducted in this experiment. Nine simulations were run by manipulating the ozone profile: 1.) 15% increase of total ozone in the profile, 2.) 15% decrease of total ozone in the profile, 3.) 30% increase of total ozone in the profile, 4.) 30% decrease of total ozone in the profile, 5.) 15% increase of total ozone above 13.5 km, 6.) 15% increase of total ozone below 13.5 km, 7.) 15% decrease in total ozone above 13.5 km, 8.) 15% decrease of total ozone below 13.5 km,.

Chapter 6 discusses the implications of the experiment design and control run. Next, there is discussion of the results of the sensitivity study that was performed. This chapter finishes with the general thoughts on how to improve future modeling studies of the TTL based on the authors findings.

CHAPTER 2

DATA

Vertical ozone profiles used for this study were gathered from observations during the NASA funded Tropical Composition, Cloud, and Climate Coupling (TC4) campaign 2007. Ozone profiles were measured using balloon borne EEC ozone sensors launched in San Jose, Costa Rica and San Cristobal, Galapagos Islands, Ecuador. A total of 28 profiles were gathered during the campaign between the two locations. An average profile with a vertical resolution of 100 m up to an altitude of 30 km was generated for each site as well as a single averaged profile which was used in the model simulations.

An updated carbon dioxide profile used for this study was generated from observational data provided by the Carbon Dioxide Information Analysis Center (CDIAC) from the station in Mauna Loa, Hawaii. Observations are collected continuously from air intakes at the top of four 7-m towers and one 27-m tower. Four air samples are collected each hour for the purpose of determining the CO₂ concentration. Determinations of CO₂ are made by using a Siemens Ultramat 3 non-dispersive infrared gas analyzer with a water vapor freeze trap (Keeling et. al. 2009).

The National Center for Environmental Prediction (NCEP) GFS 1° global model analysis data is used to generate a prescribed average sea surface temperature (SST), imposed background vertical motion profile, and average tropical sounding. Profiles were created by taking a one month average (July 15th – August 15th, 2007) of temperature, water vapor, vertical motion, and SST data inside a virtual grid box extending from the Equator to 9°N

latitude and 85.5°W to 106°W longitude. The size and location of the grid box were chosen for two reasons. First, the virtual grid box covers the general area of the Eastern Pacific Ocean as was studied by NASA's TC4 campaign, where extensive in situ atmospheric observations were gathered during the one month time span. Secondly, the grid box needs to encompass the effects of the background vertical motion associated with deep convection apart of the ITCZ and associated subsidence outside of convective regions.

CHAPTER 3

MODEL DESCRIPTION AND EXPERIMENT DESIGN

In order to complete this modeling study to investigate the formation of the TTL and favored generation regions of TTL cirrus, the University of Wisconsin Non-hydrostatic Modeling System (UW-NMS) is used. The UW-NMS described by Tripoli (1992), is a three dimensional cloud resolving model that can be used to investigate processes at a large range of scales from hemispheric to micro- β . It uses a non-Boussinesq and quasi-compressible framework, and it is built to conserve enstrophy as well as kinetic energy against three dimensional numerical sources and sinks.

The UW-NMS utilizes a comprehensive mixed-phase microphysics parameterization. This two moment bulk scheme predicts mixing ratio and number concentration of rain, graupel, snow, hail, pristine crystals, and aggregates. A complete description of the bulk microphysics scheme can be found in Flatau (1989). The radiation scheme employed by the UW-NMS is the Rapid Radiative Transfer Model (RRTM). Readers are referred to Mlawer (1997a) and Mlawer and Clough (1997b) for details about the respective longwave and shortwave radiation schemes and validation experiments.

3.1 Experiment Design

Model runs were done in a quasi-2d framework. This involved using 3 grid points in one horizontal direction, while retaining the full 1,000 by 60 grid points in horizontal and vertical directions. The second horizontal dimension is not fully eliminated to allow for a more realistic treatment of boundary conditions and fluxes out of the model grid. Model

resolution in the horizontal directions is set to 1 km and the vertical resolution is uniformly set to 500m.

Model simulations include periodic boundary conditions in the horizontal directions and a Rayleigh Friction “sponge” layer is placed at the upper portion of model grid which serves to prevent upwardly propagating waves from being refracted back into model space rather than being let out of the top of the model boundary. Particular attention was paid to the depth of the sponge layer. The base of the dampening layer needs to be high enough so that UTLS dynamics remain unaffected by the layer, and it must be deep enough from the top of the model grid to inhibit artificial model generated wave breaking and subsequent mixing. After a series of short experiments to fine tune the theory above, the depth of the sponge layer was set to 8 km with its base at 22 km.

The model domain surface is set to tropical ocean with a prescribed sea surface temperature (SST) of 305 K. An imposed background vertical motion tendency, shown in Figure 2, is added to the model’s advection scheme to replicate a mean upward motion within the ITZC region and associated tropical Hadley Circulation. This profile is suggestive of upward vertical motion in a tropical wave by prescribing a convergence/divergence profile normal to the 2-d plain. It is important to state here that while a particular profile was made based on the location of grid box (Tropical Eastern Pacific) described in the Data section, the experiment design is set so that the size and location of the grid box and resulting vertical motion profile can be altered to study properties of the TTL in different tropical locations.

A one week averaged tropical sounding including temperature, moisture, and wind profile including shear (Figure 3) was used to initialize the model control run and stimulate convection. This averaged tropical sounding was generated using NCEP 1° GFS model

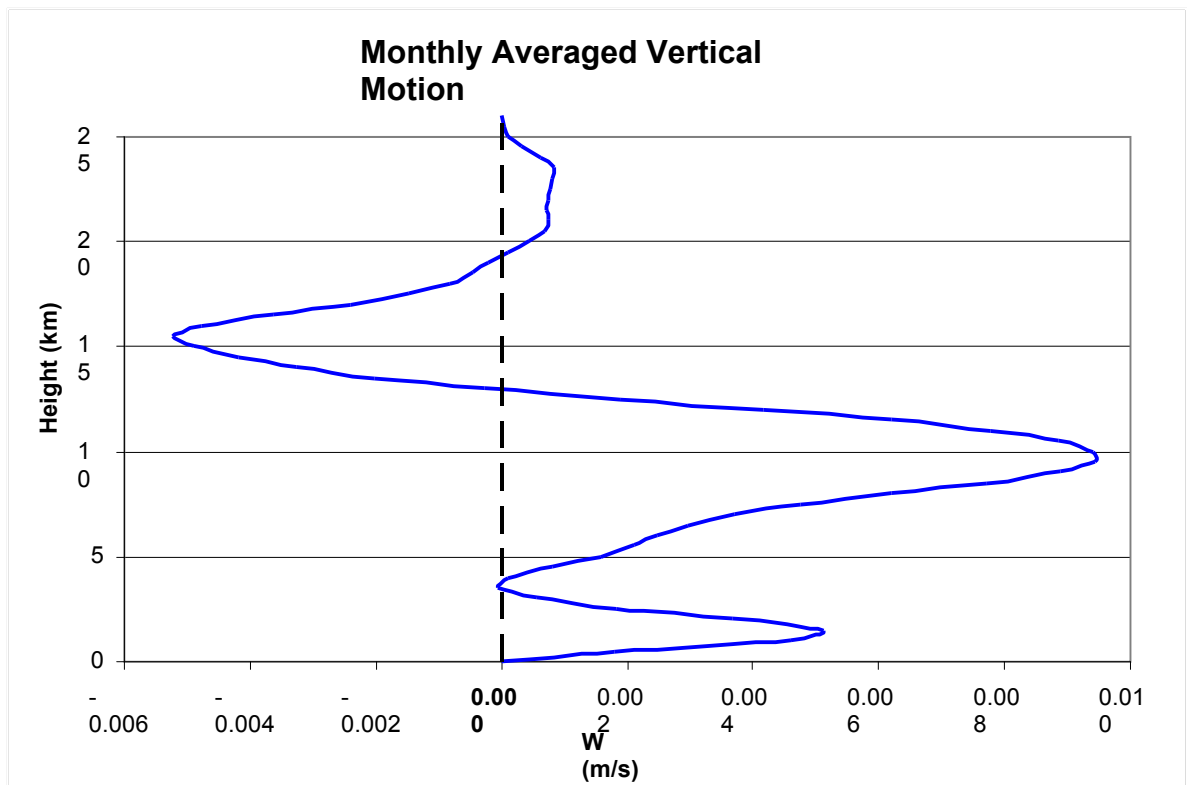


Figure 2: Average vertical motion vs. height using NCEP GFS 1° global model analysis data. Profile was created by taking a one month average (July 15th – August 15th, 2007) inside a grid box extending from the Equator to 9°N latitude and 85.5°W to 106°W longitude.

analysis data inside a virtual grid box extending from the Equator to 9°N latitude and 85.5°W to 106°W longitude, matching the location of prescribed avg. SST and background vertical motion profile. The moisture profile was altered so that all water content above ~600 hPa was removed. Thus, convection and mean large scale ascent (tropical upwelling) are left to vertically transport water vapor into the upper UTLS. The tropical ozone profile used in the control run is shown in Figure 4. This profile was generated using data from the 2007 TC4 campaign as discussed in Chapter 2 and is also representative of the virtual grid box explained above. Carbon dioxide is taken to be well-mixed and so is described by a single mixing ratio; for all experiments a 2007 averaged value of 383 ppmv is used.

The RRTM radiation scheme is used for all modeled simulations in the longwave and shortwave bands. The radiation profile is updated every 3600s during all model runs. The longitudinal variation of incoming shortwave radiation is turned off and set to a fixed date (early August). Therefore, the 24 hour diurnal cycle in shortwave and longwave radiation still exists, but the position of the sun in relation to the earth and its radiative effects do not change. This is done in order to help the model reach radiative convective equilibrium since model spin up time is on the order of 2-3 months. Similar techniques are employed in other CRM studies of the TTL (e.g. Kuang and Bretherton, 2004).

This experiment design is loosely based on earlier work by Tripoli (1992) and Grabowski et al. (1996). These earlier modeling studies were designed to investigate the long term behavior of precipitating tropical cloud systems. They were successfully able to simulate a single continuously propagating tropical squall line with multiple towers after the first simulation week that would propagate from east to west. Convectively driven subsidence opposed prescribed upward vertical motion outside of the squall line and they

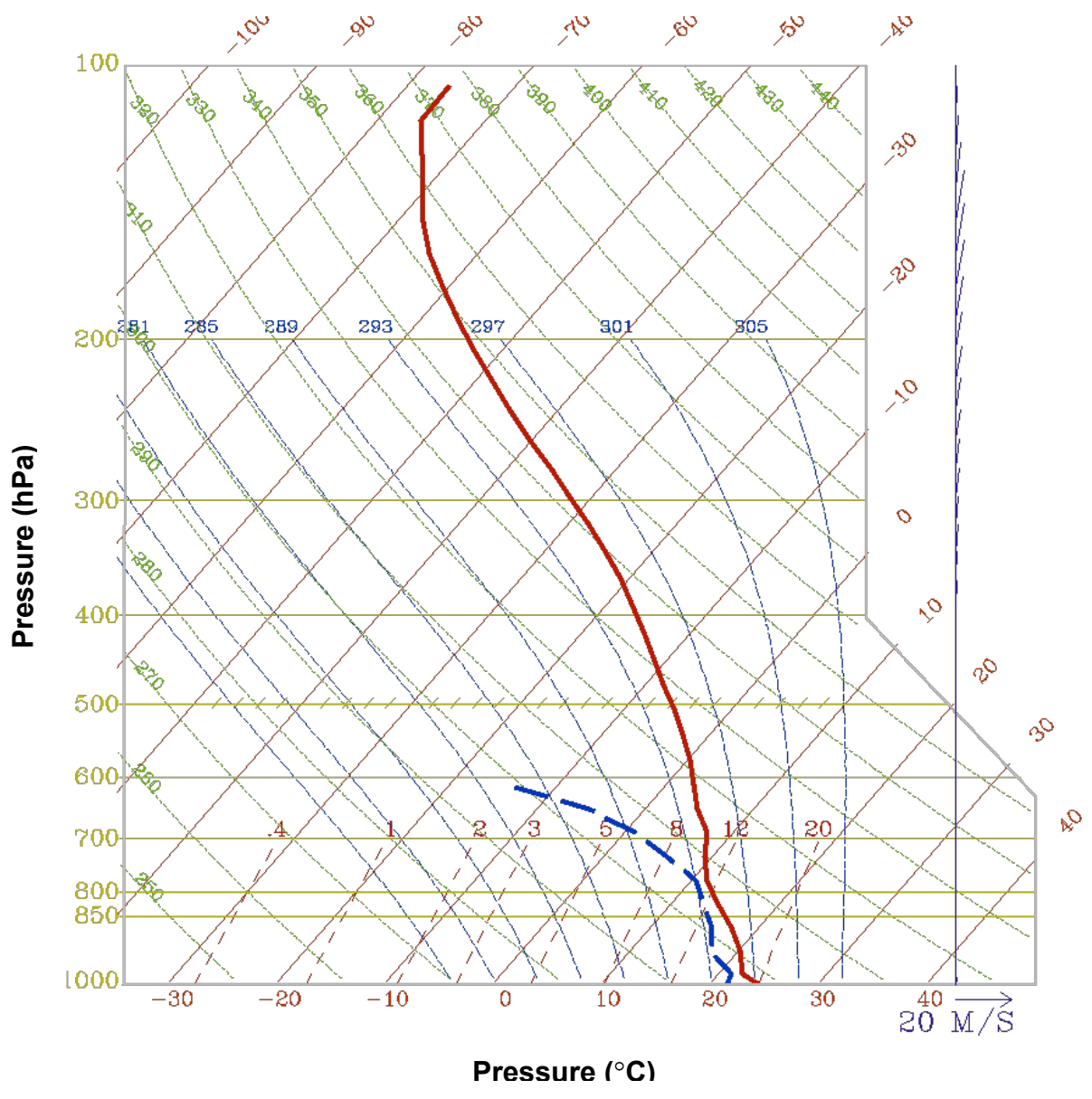


Figure 3: Skew-T diagram of tropical sounding used to initialize the model. The Sndplt program was used to generate this skew-t. The vertical axis is pressure in (hPa) and the horizontal axis is temperature in (°C). The thick solid red line is the temperature profile. The thick dashed blue line is the moisture profile. The purple vertical axis on the right displays the wind speed and direction at each level in (m/s). Green lines sloping from upper left to lower right are constant potential temperature (°K). Thin red lines sloping from right to left are isotherms (°C). Dashed thin red lines are constant mixing ratio (g/Kg). Light dashed blue lines are moist adiabats (°K).

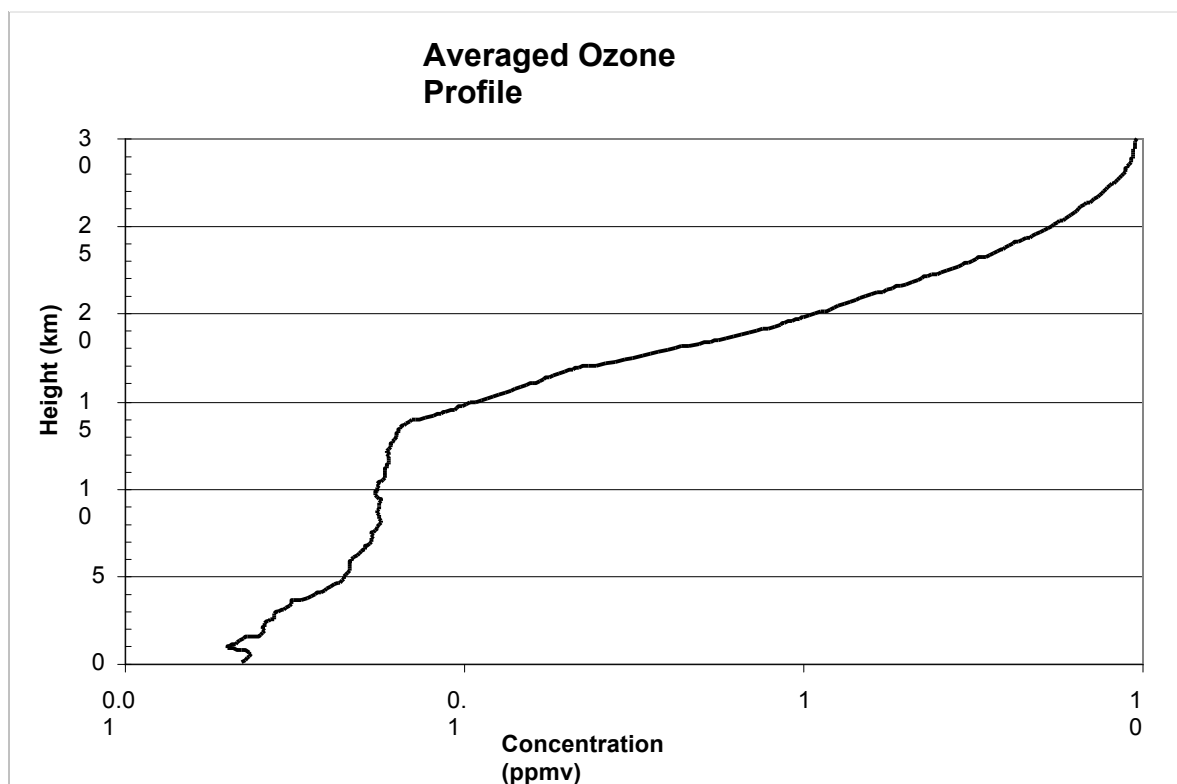


Figure 4: Averaged ozone profile vs. height. This profile was generated using observational data from balloon borne ozonesondes launched during the TC4 campaign in San Cristobal, Galapagos Islands and Alajuela, Costa Rica.

also found that a trailing anvil was formed which mostly dissipated before completely wrapping around the model domain. The experiment design for this model study is set up in order to be able to reach a radiative convective equilibrium within the model domain and replicate the deep convective features of these earlier studies, while putting primary focus on examining the maintenance and variability of the TTL and associated dynamical, radiative, and microphysical processes within the region.

CHAPTER FOUR

CONTROL EXPERIMENT

As was stated in the introduction, the goal of this modeling study is threefold: to fulfill the experiment design to successfully simulate the formation and maintenance of the tropical tropopause layer from an initial dry tropical sounding including shear, to replicate the types of observations seen during field programs and previous research, and to examine the sensitivity of this layer to various important species and processes within the region. The control run was set up based on the experiment design in order to validate the first two goals and then based on these results conduct sensitivity experiments that are tailored to the results. The control simulation ran for 142 days and the results from this run are covered in the following two sections.

4.1 Radiative-Convective equilibrium

The control run reaches RCE after ~100 days. Then, the model was run for another six weeks after RCE to study various processes occurring within the domain and in particular, the TTL region. In order to verify the model reaching RCE, the model domain averaged temperature and vertical motion are sampled every time step (8 sec) and then averaged every hour. This is done every kilometer from 7-17 km (Fig 5, shows 8 km and 15 km). It is important to note that in CRM simulations the RCE achieved is a statistical equilibrium where temperature continues to fluctuate. The author refers the reader to Kuang and Bretherton (2004) for further details on the theoretical underpinnings.

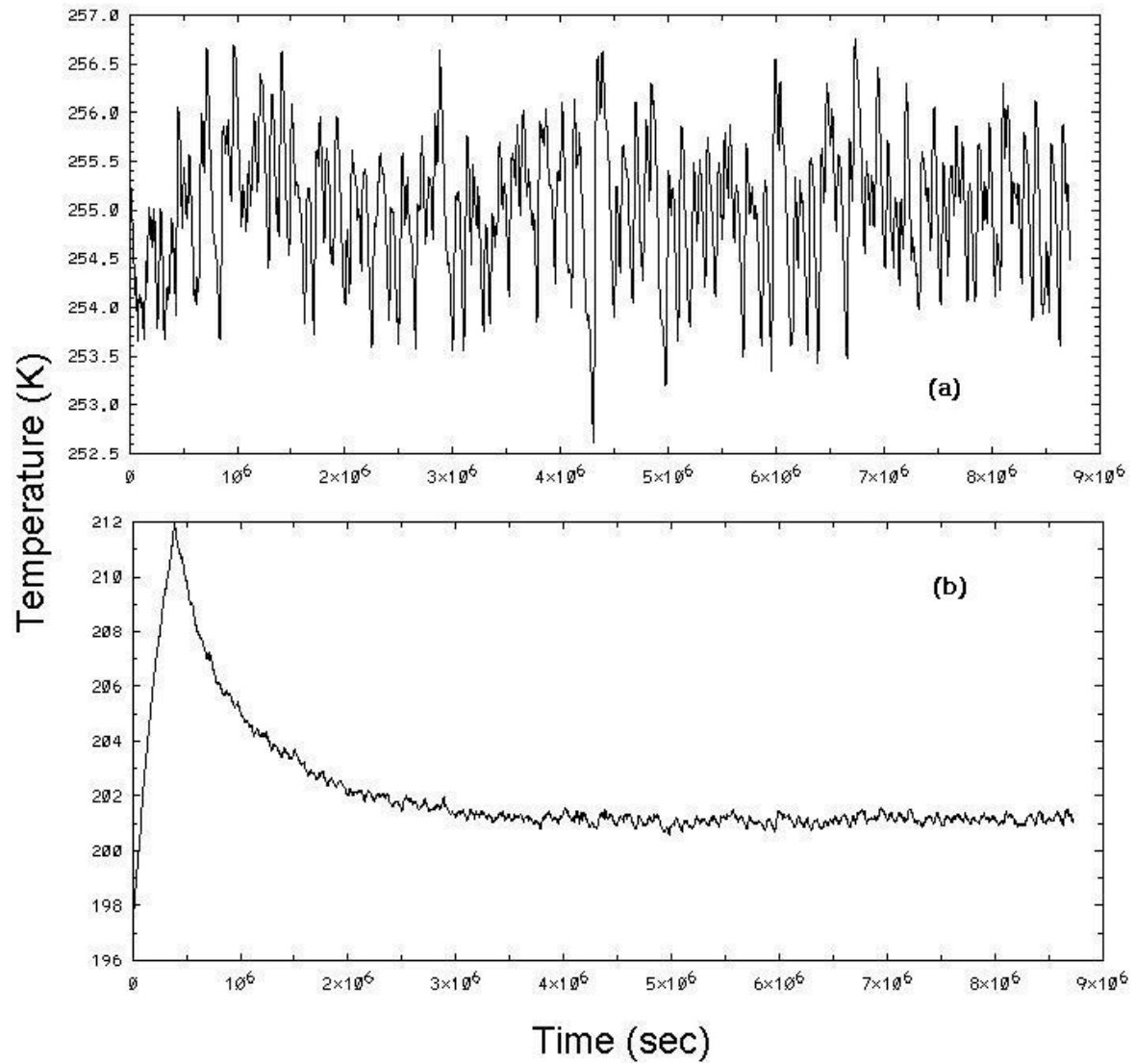


Figure 5: Domain averaged temperature fluctuations. (a) at 8 km and (b) at 15 km over the first 100 days of the control simulation. The values are sampled every time step and 1 hr averages are shown.

In Fig. 5 at 8 km (a), temperatures in the middle troposphere fluctuate ~ 2.5 K peak-to-valley on very short time scales due to convection and/or gravity waves. A ~ 1 K peak-to-valley fluctuation on a much longer time scale (~ 30 days) is clearly evident and is explained as a radiative response to convective induced cooling (Kuang and Bretherton, 2004). At 15 km (b) in Fig. 5, significant warming of 14 K occurs over the first 6 days. Then pronounced cooling in the TTL which ultimately settles at an equilibrium temperature of ~ 201 K. Small temperature fluctuations of 0.5-1 K peak-to-valley can be seen on a longer time scale around 20 days similar to that which is seen in the bulk troposphere. All results shown in the following section are gathered after the simulation has reached RCE (100 days) and all data gathered before RCE is not used, as it is considered part of the model spin up.

4.2 Control Run Results

As was previously stated the control simulation was run for another six weeks after reaching RCE. Most figures shown below will feature domain averaged data sets from the first three weeks beyond RCE. This is done in order to present the control run data that will be used as the background state in the subsequent sensitivity experiments.

Figure 6 shows the domain averaged temperature, potential temperature, and equivalent potential temperature profiles after 121 days in the control simulation. In the boundary layer, a surface temperature of 300.6 K (27.5 C) and a surface water vapor mixing ratio of 18.01 g/kg is maintained by surface fluxes off the prescribed ocean surface with uniform SSTs set to 300.5 K. These values are similar to those observed over the north equatorial eastern Pacific and western Pacific warm pool. The average boundary layer θ_e is 348.8 K (Fig 6c.) which is above the 345 K threshold at which air parcels first attain positive

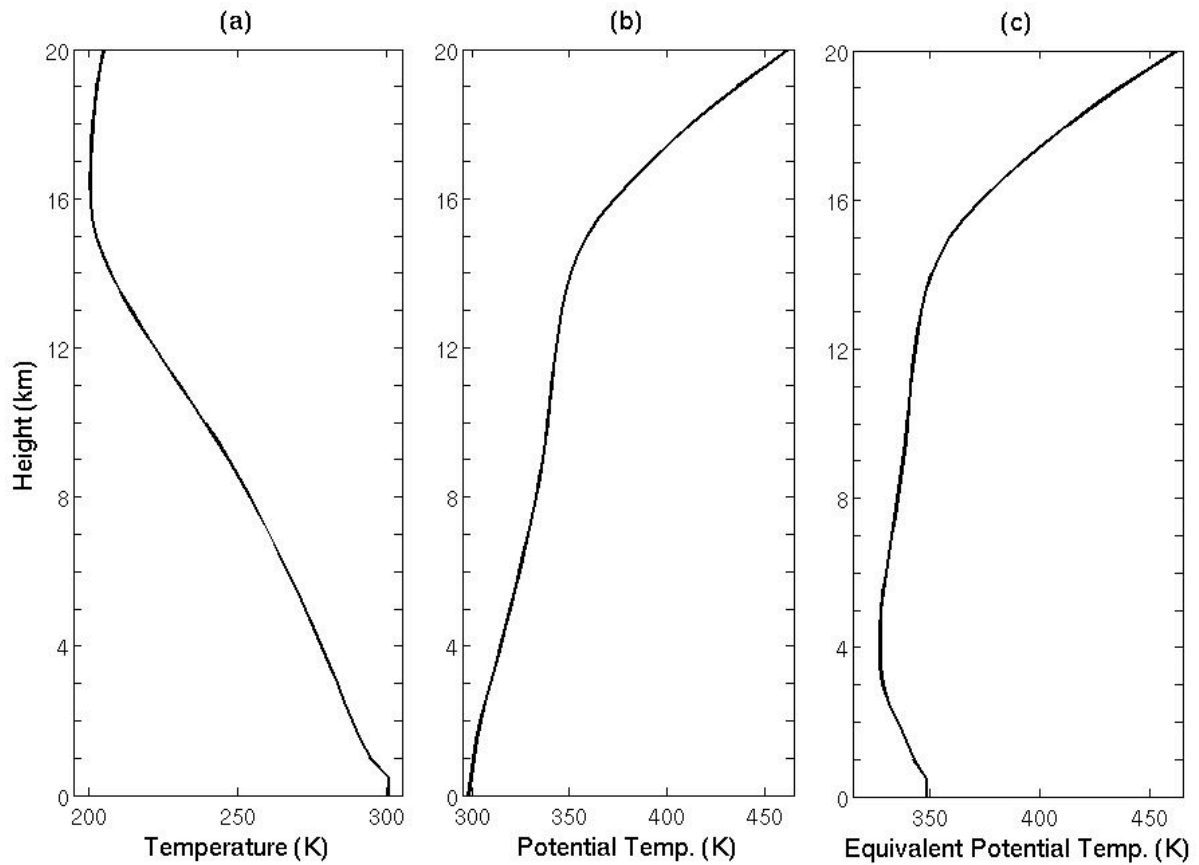


Figure 6: Vertical temperature profiles gathered from the control run. (a) Averaged temperature profile (K) vs. height (km). CPT is located at approximately 16.5 km with a temperature of 200.8 K. (b) Averaged potential temperature profile (K) vs. height (km). (c) Averaged equivalent potential temperature (K) vs. height (km). A sharp increase in θ and θ_e is evident above 16 km associated with highly stable stratosphere above.

CAPE, and may participate in convection (e.g. Folkins et al., 2002). Typical convection initiated within the boundary layer with this value of θ_e would be capable of reaching and detraining to around 13.6 km based on corresponding upper troposphere θ_e values, with some turrets potentially overshooting their LNBS. In the upper troposphere, the CPT is clearly seen in the temperature profile and located at 16.5 km (105 hPa) with a temperature of 200.8 K. Evidence of the stratospheric inversion mainly induced by warming from ozone is clearly evident above 16 km in both the potential temperature and equivalent potential temperature profiles.

Figure 7 shows the vertical profiles of ozone concentration and averaged atmospheric lapse rate. There are several key features to notice in this figure. The temperature profile is conditionally unstable throughout the bulk troposphere and moist-adiabatic throughout a deep layer in the troposphere which are both reflected in typical tropical soundings. The lapse rate profile is in good agreement with soundings launched from San Cristobal located in the Galapagos Islands during the 2007 TC4 campaign. The traditional lapse rate tropopause can be seen around 16.5 km coincident with the CPT. The LRM is located at ~10.5 km (275 hPa) and in a general region from 10-12 km. The LRM is co-located with the O_3 min in the ozone profile in the middle troposphere and also located below the vertical mixing barrier (13.5 km). These results are consistent with the results from previous studies linking the LRM and O_3 min to the vertical mixing barrier (e.g. Folkins et al., 1999; Gettelman and Forrester, 2002). The vertical mixing barrier lies approximately at the same height (13.5 km) as detraining typical convection with a surface equivalent potential temperature of 347.2 K (Fig. 5) or the LMCO.

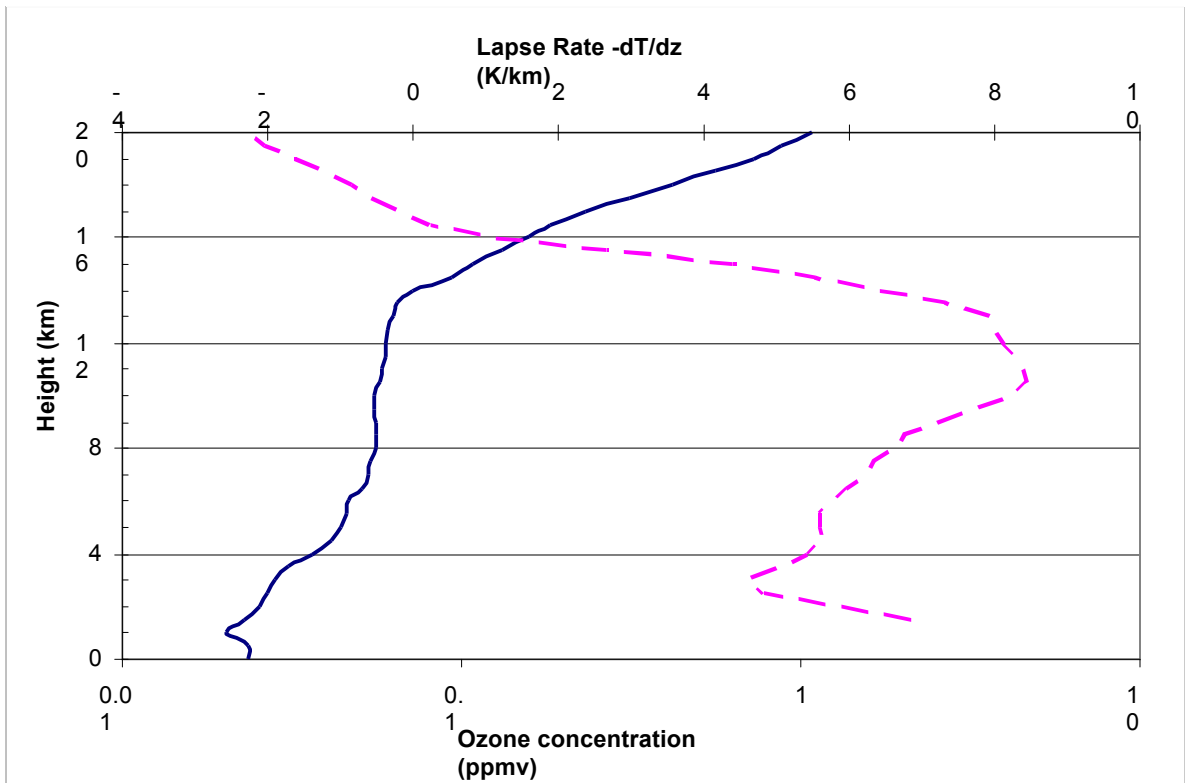


Figure 7: Plot of tropical ozone profile and averaged atmospheric lapse rate vs. height (km) from the control run at 121 days. The solid blue line is the ozone concentration in (ppmv). The dashed pink line is the atmospheric lapse rate $-dT/dz$ in (K/km). This figure highlights the connection between the LRM and O3 min as can be seen from 10-13km. The vertical mixing barrier can be seen in the ozone profile beginning above 13.5km.

Convection occurs frequently within the bulk troposphere throughout the control simulation. There are active convective periods with organized tropical squall line systems that traverse from east to west across the domain that last on the order of 8-12 hrs, and there are also quiet periods without active convection. Most of the unorganized convection and subsequent anvils do detrain around the LMCO (13-14 km). As the convective towers subside, large (200-500 km) trailing anvils can be seen lingering around the LMCO for several hours. As expected, much of the ice particles in the anvils sediment out in the subsiding regions outside of convection updrafts. These results mimic previous work (e.g. Tripoli, 1992; Grabowski et al., 1996) used to develop the experiment design for this study.

Figure 8 shows the net heating profiles including both shortwave and longwave contributions for ozone, water vapor, carbon dioxide, and the total radiative profile in the TTL region. Given that much of this region above the LMCO is typically higher than most convection, the radiative properties of various chemical species largely determine the sign of the heating profiles. Ozone is a large net heating source in the TTL (~ 0.3 K/day) especially above the vertical mixing barrier where concentrations begin to grow exponentially. In the lower stratosphere the heating rate grows to 1-2 K/day and throughout the UTLS is positive in both the longwave profile and shortwave profile (not shown).

Water vapor is largest contributor to radiative cooling in the bulk troposphere and in the TTL region. The net contribution of water vapor in the TTL region is cooling around -0.2 K/day. In the bulk troposphere (not shown) longwave cooling by water vapor is on the order of -1.5 K/day. In the shortwave profile the net heating rate is positive ~ 0.3 K/day, although this is an order of magnitude less than its longwave contribution.

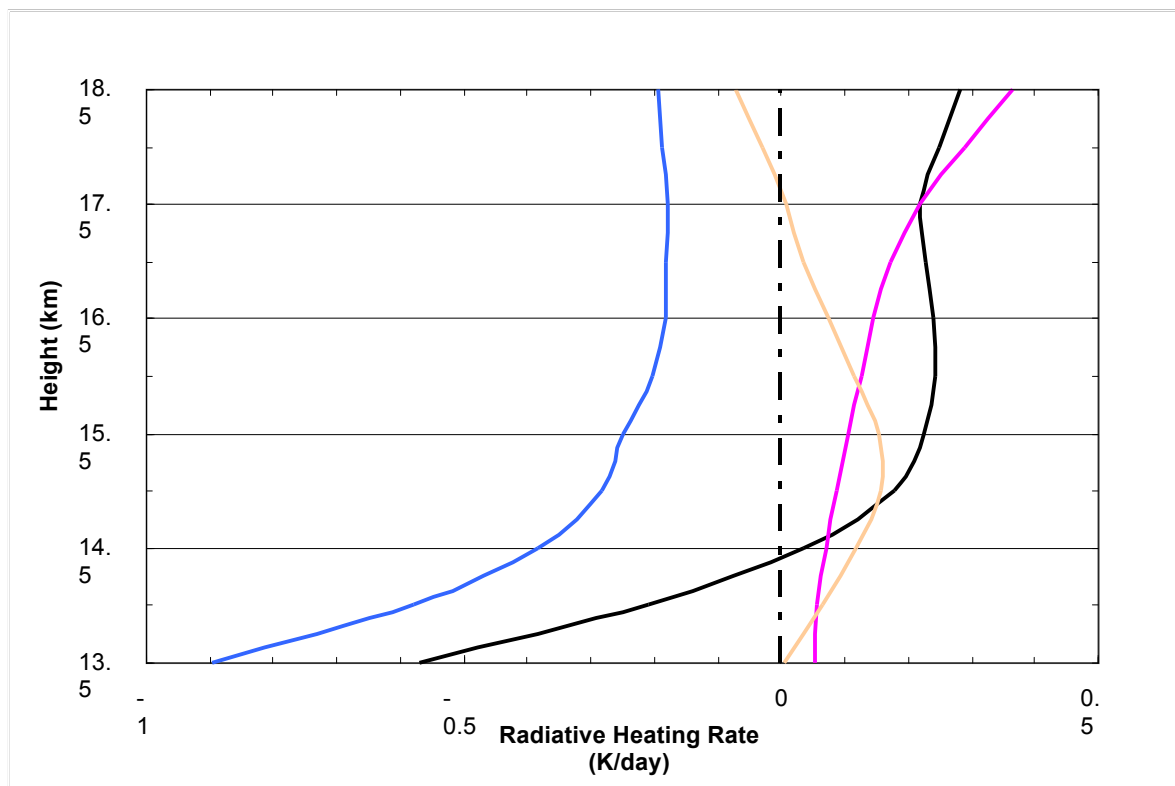


Figure 8: This plot shows net (LW + SW) heating rates of important chemical species in the TTL region in the control simulation. The solid black line is the total radiative heating rate. The solid blue line is the net water vapor heating rate. The solid tan line is the net carbon dioxide heating rate. The solid pink line is the net ozone heating rate. The dashed black line marks, $Q=0$.

Carbon dioxide plays a smaller role in the radiative spectrum throughout the bulk troposphere. However, in the TTL region where water vapor concentrations become very small, carbon dioxide plays a crucial role. It is a source of net heating around 0.1 K/day and combined with ozone it largely balances the cooling from water vapor.

The final profile plotted in Fig. 8 is the total net radiative heating rate in the TTL region in the control run. As was stated earlier long wave cooling by water vapor dominates in bulk troposphere and thus the total net heating rate is negative (~ 0.25 K/day) until around 14.4 km where the sign of the heating changes sign (LZRH). Above this level where heating from ozone and carbon dioxide dominate cooling by water vapor, the total net radiative heating rate is around 0.25 K/day. This positive net radiative heating comprises the lower reaches of the Brewer Dobson circulation, which largely modulates the strength and seasonality of mean tropical upwelling. Finally it is important to note that the mean radiative heating rates found in the control run largely mimic those in previous studies (e.g. Gettelman et al., 2004; Fueglistaler et al., 2009).

In order for convection to transfer air to the stratosphere it must either penetrate directly into the stratosphere, which is shown to occur on rare occasions in the tropics (e.g. Danielson, 1993; Fueglistaler et al., 2009) or convection must transport air above the LZRH where mean tropical upwelling can loft the air through various radiative processes e.g. cirrus lofting, diabatic ascent, etc. (Sherwood, 2000; Corti et al., 2005; Corti et al., 2006). Figure 9 displays the averaged total radiative heating rate including the shortwave and longwave contributions in the control run. The LZRH is found at 14.4 km (149.2 hPa) and the potential temperature is 353.9 K. These results are in good agreement with Corti et al. (2005) where

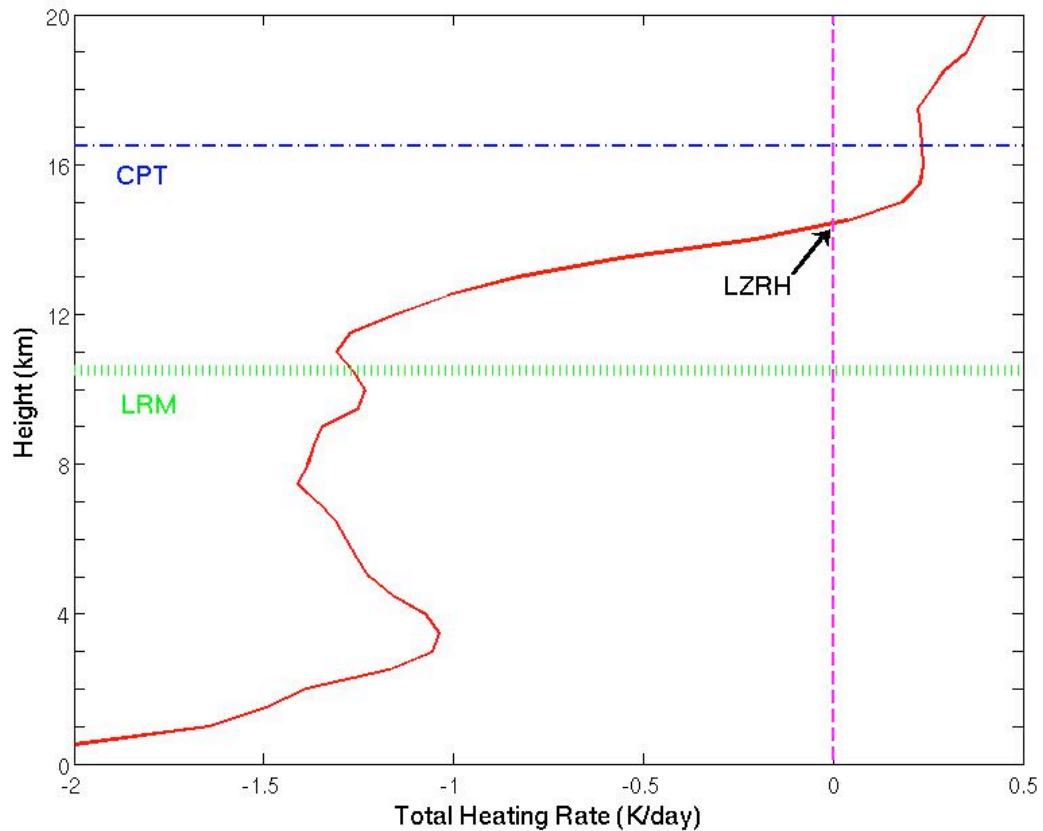


Figure 9: Plot of the averaged radiation profile from the control run. The x-axis is the total heating rate (K/day) including both the shortwave and longwave contributions, and the y-axis is height (km). The LZRH is located at ~ 14.4 km (353.9 K, potential temperature) above this level air is radiatively heated towards the CPT and stratosphere above, and below this level radiational cooling dominates as air will sink back into the lower troposphere. The red solid line is the total averaged radiation profile. The dashed pink vertical line marks, $Q=0$. The green hatched line is the LRM at 10.5 km. The blue hashed-dotted line marks the CPT at 16.5 km.

the transition from radiative cooling to heating occurs about 1.5-1.0 km lower in full sky type conditions versus clear sky conditions.

While most convection in the control simulation detrains at the level of main convective outflow, stronger convective cores overshoot their LNB, can penetrate above the LZRH, and even penetrate above the CPT into the lower stratosphere. Figure 10 shows an example of a rare deep convective event that detrains to around 15.5 km. This figure also depicts a convective turret overshooting its LNB directly into the lower stratosphere to 17.8 km. This image was gathered from the control run at time 9784800s (~113 days). Strong surface fluxes off the ocean increased boundary layer equivalent potential temperatures to ~351 K, with a corresponding detraining height based on parcel theory to around 15.5 km. Surface based CAPE is around 2,500 J/kg, providing an maximum overshoot of over 2.5 km. Above 6-8 km much of the convective core and anvil is made up of pristine crystals (Fig 10b), snow, aggregates, and super cooled water. The horizontal extent of the trailing anvil is around 300 km most of which is approximately above 14.5 km (above the LZRH). As is seen in Fig 10c, this type of rare deep convection can have a direct moistening effect in the lower stratosphere as water vapor concentrations around 15 ppmv are injected above 17 km.

Ubiquitous cirrus clouds are present in the TTL region during the control simulation. Most of the cirrus appear to be generated by detrained ice crystals from convective anvils around 13-15 km. The larger ice crystals with higher fall speeds tend to sediment out hours after detrainment but smaller crystals linger in the TTL for extended periods of time (>12 hrs). It was shown in the results that supersaturations with respect ice and subsequent homogeneous pristine ice crystal formation are occurring not only in updrafts associated with convection, but also by in-situ formation outside of convective events. Figure 11 shows an

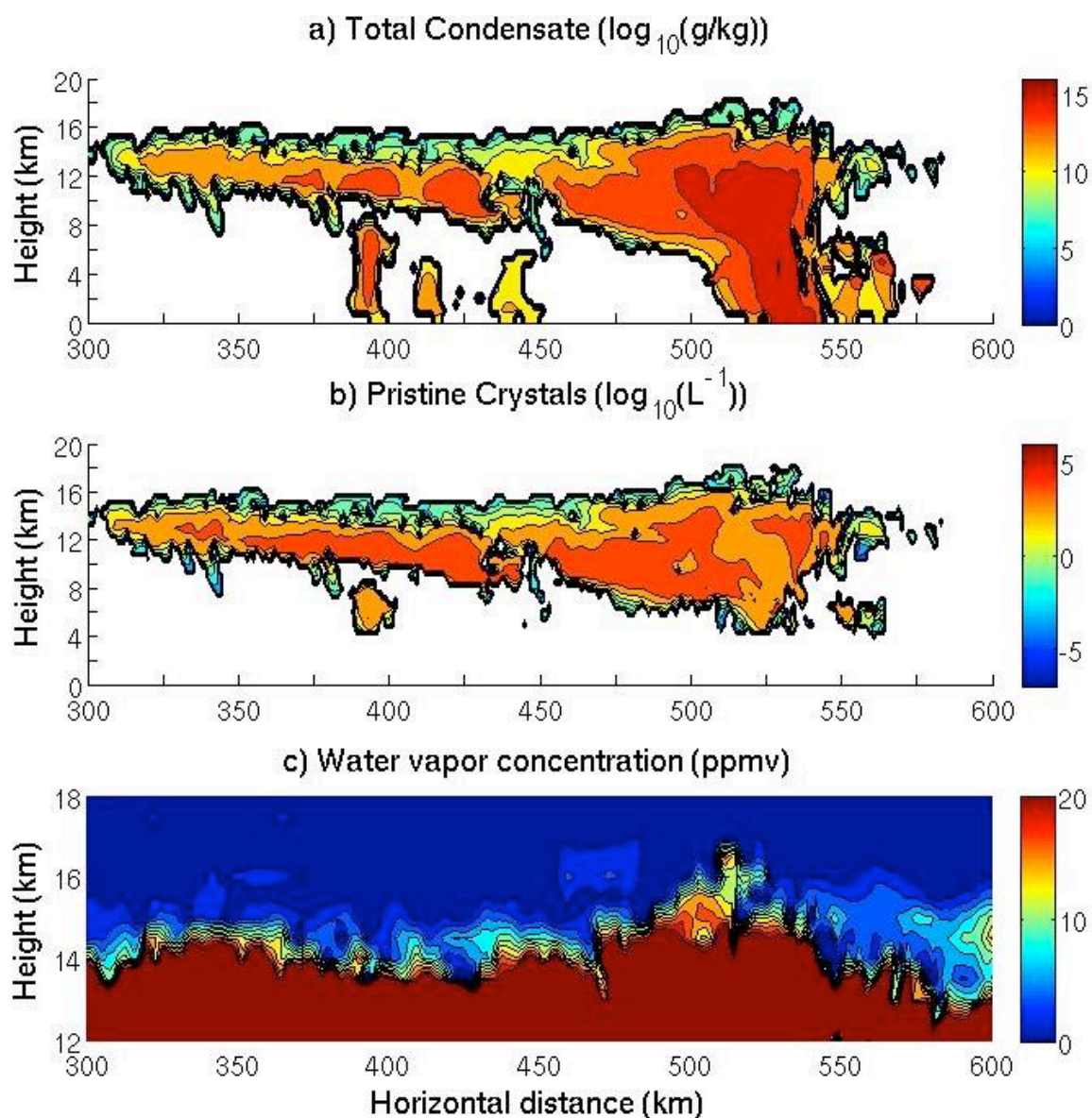


Figure 10: Deep convection penetrating the CPT and into the lower stratosphere. a) Shows total water condensate from water vapor, snow, ice and aggregates vs. height. b) Shows pristine ice crystal concentrations per liter vs. height. c) Shows the water vapor concentration vs. height. This deep convective event is evidence in the model control run of deep convection directly hydrating the lower stratosphere. The overshooting top emphasized in c) reaches 17.2 km.

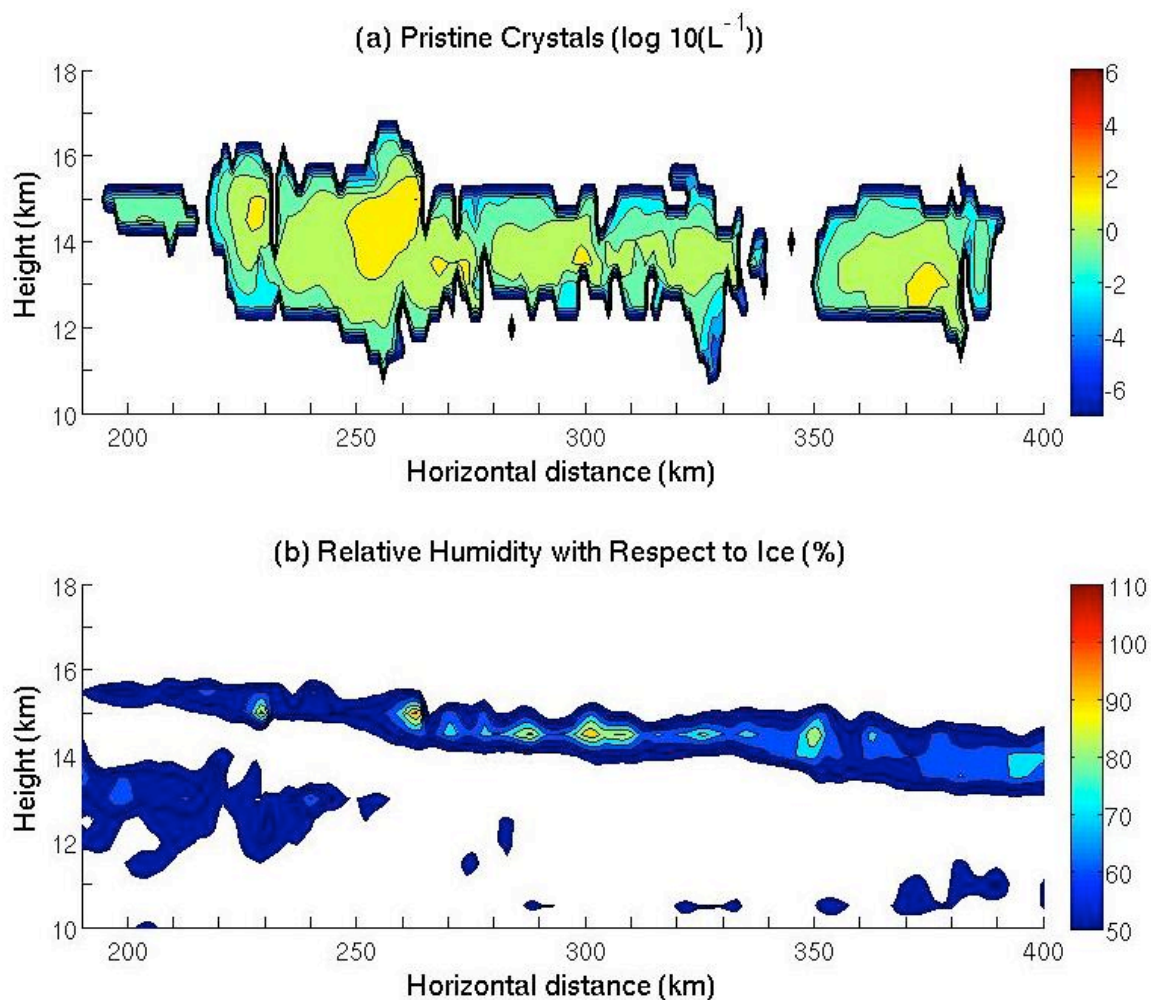


Figure 11: TTL cirrus from control experiment at 8694000s. a) Plot of pristine ice crystal concentration vs. height. b) Plot of relative humidity with respect to ice vs. height. TTL cirrus generated from detrained convective anvil located in the model domain. There is a small region of supersaturation with respect to ice where pristine ice crystals can continue to grow homogeneous nucleation.

example of a TTL cirrus within the model domain of the control run. This cirrus is smaller in horizontal size (~200 km) and located around 14.5-15 km. The pristine ice concentration in the center of the cloud is around 1 per liter. When looking at b) it is evident there is a small region that is above 100% relative humidity with respect to ice, and this is where new pristine ice crystals can grow by homogeneous nucleation. Given the small area of supersaturation with respect to ice, this cirrus does not last long as many of the ice crystals sediment out over the following 5 hrs in the control simulation. This cirrus is outside of convective activity and is thus formed by the in-situ mechanism.

Figure 12 shows the vertical domain averaged water vapor concentration profile at the beginning and end of the control run. Fig 10b shows a close up of the water vapor concentration in the TTL region and in particular at the CPT. The average water vapor concentration in the TTL is around 3.5-7 ppmv and the water vapor concentration at the CPT is ~1.2 ppmv. This value is similar to observational data from various previous studies, but on the low end of the range. It is important to note again that issues with observational data due to biases between instruments used to measure concentrations is still largely unresolved (Kley et al., 2000). The major point to take away from Fig.12 is that deep convection and subsequent tropical upwelling have taken and initially dry TTL and moistened it to near observational values.

4.3 Summary

The experiment design of the control run fulfills the modeling goals of this study. The control simulation reaches a statistical RCE after ~100 days. The control run successfully simulates the TTL and its critical levels. The LRM is found to be at ~10.5 km (275 hPa) and coincident with the LRM is the O3 min. The LMCO is found to be around the vertical mixing

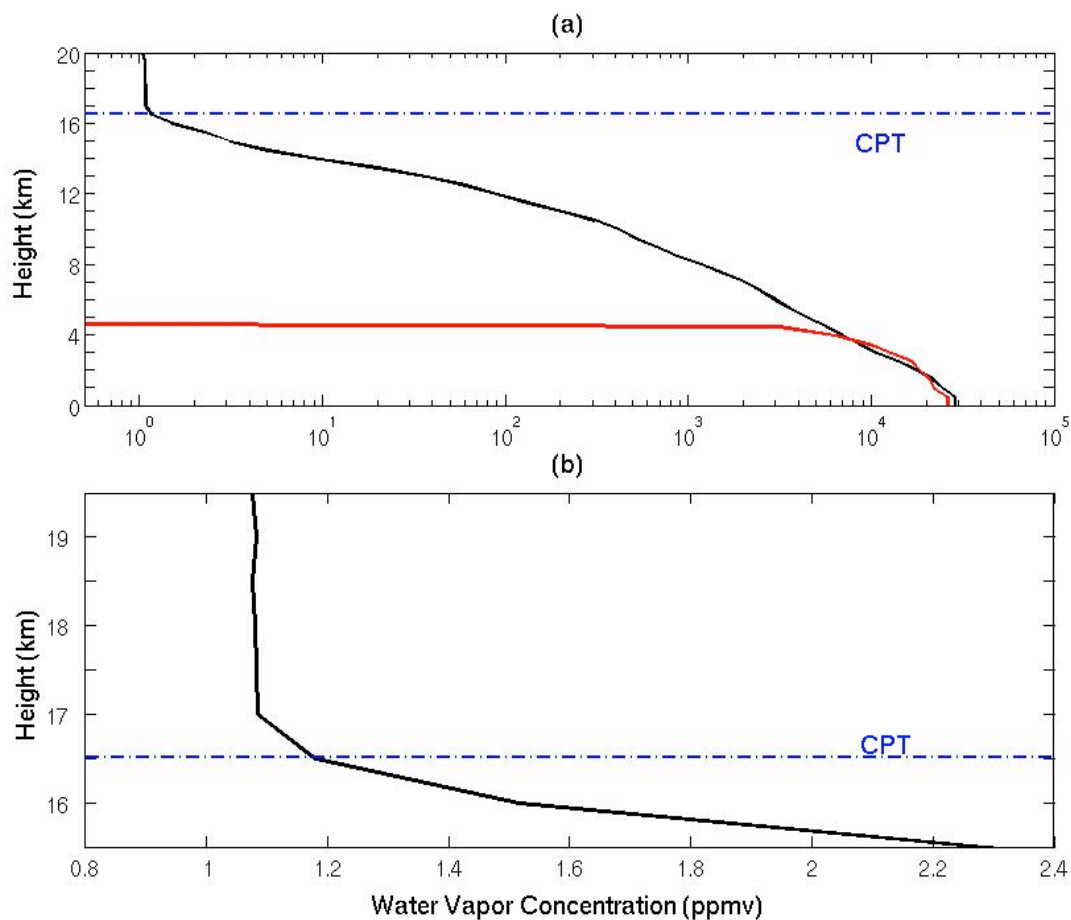


Figure 12: Plot of average water vapor profiles from the control run, (a) water vapor concentration (ppmv) in log scale vs. height (km) in the vertical. Black solid line is the averaged water vapor concentration at 121 days. The solid red line is the initial water vapor profile at 0 days. (b) is same as (a) but zoomed in to the upper TTL region. Dashed blue line denotes the CPT. The average water vapor concentration throughout the TTL region is around 3.5-7 ppmv and 1.2 ppmv at the CPT.

barrier at ~ 13.5 km. The LZRH is located at 14.4 km (150 hPa) and at a potential temperature of 353.9 K. Above this point air is lifted by diabatic ascent and has the potential to reach the lower stratosphere. The CPT is found at ~ 16.5 km (105 hPa) at a temperature of 200.8 K. These levels match well with observational data and previous studies.

Convection occurs frequently in the control run. There are active and quiet convective periods. Organized tropical squall lines develop that last 8-12 hrs and there is also unorganized convection. Mean subsidence prevails in the bulk troposphere outside of convective towers. Most convection detrains at the LMCO around 13-14 km, but there is evidence of stronger convective updrafts overshooting there LNB into the TTL and above the LZRH. Several deep convective events penetrate above the CPT and into the lower stratosphere.

Ubiquitous TTL cirrus clouds are present in the TTL region during the control simulation of which most appear to be generated by detrained ice crystals from convective anvils around 13-15 km. These cirrus can persist due to supersaturations with respect ice and subsequent homogeneous pristine ice crystal formation. There are also TTL cirrus that form in-situ outside of convective events. The simulation is unable to fully resolve the presence SVC formation (thickness ≤ 500 m) given the vertical resolution and bulk microphysics used.

This CRM study is different than previous studies in that effects of shear were not removed from the initial tropical sounding. Thus, this simulation is a more realistic treatment to gravity waves shed from convection. After inspection of the potential temperature field, there was no evidence found of gravity wave breaking and therefore no induced cooling or heating. This design also allows for the inclusion of longer time scale stratospheric features (e.g. QBO). All water vapor above ~ 600 hPa in the averaged tropical sounding was removed

in order to determine if a combination of deep convection and large scale upwelling could transport enough water vapor into the TTL in the simulation to match observational data and previous studies. The average water vapor concentration in the TTL is around 3.5-7 ppmv and 1.2 ppmv at the CPT. These values are similar but on the low end of ranges to values gathered through observational data. The final portion of this modeling study involves running a series of sensitivity experiments to test how receptive the TTL is to changes in concentration of the mean ozone profile.

CHAPTER 5

SENSITIVITY EXPERIMENTS

Further insight into the mechanisms determining the temperature structure of the TTL in the UW-NMS model can be obtained through sensitivity experiments. The concentrations of ozone in the averaged tropical profile is modified over a range of values; for each value the model was reinitialized at RCE (100 days) as discussed in Chapter 4 and run for another 21 days to a new equilibrium. The domain averaged temperature and height of the CPT and LZRH are diagnosed, along with the radiative heating contributions from relevant species.

5.1 Sensitivity to ozone

In the sensitivity experiments, the concentration of ozone in the tropical profile was varied. Four subsets of experiments were performed. In the first subset, the ozone concentration through the entire profile was increased and then decreased by 15%. In the second subset, the ozone concentration through the entire profile was increased and then decreased by 30%. After learning about the importance of the vertical gradient in ozone or vertical mixing barrier from various studies (e.g. Folkens et al., 1999; Gettelman, 2002), the next two subsets of experiments were implemented. Fig. 4 displays the tropical ozone profile used in the control run. The start of the large vertical gradient in ozone is located at approximately 13.5 km. In the third subset, the ozone concentration above 13.5 km was increased and then decreased by 15%. In the fourth subset, the ozone concentration below 13.5 km was increased and then decreased by 15%. In the first four subsets of experiments, the ozone profile remains fixed in time. The following sections (5.1.1-5.1.4) will present the

results of the sensitivity study and the final section (5.2) will summarize these results and provide some brief discussion.

5.1.1 O₃ ppmv +/- 15% entire profile

In the first subset of experiments, the ozone concentration was increased and then decreased by 15% and compared to the control results. Figure 13a shows the averaged temperature profiles from these two experiments and the control run. It focuses in on the TTL and in particular the CPT. A 15% increase ozone across the entire profile lowers and warms the CPT to 16 km (114.9 hPa) with a temperature of 201.2 K. A 15% decrease in ozone raises and cools the CPT to 17 km (96.9 hPa) with a temperature of 200.6 K. Figure 13b shows the averaged net radiative heating profiles from these two experiments and the control run. A 15% increase in ozone causes the LZRH increases to 14.8 km (141.6 hPa) and the potential temperature at this level increases to 357.1 K. While a 15% decrease causes the LZRH slightly increases to 14.5 km (148.2 hPa) and the potential temperature decreases to 353.3 K.

5.1.2 O₃ ppmv +/- 30% entire profile

In the second subset of experiments, the ozone concentration was increased and then decreased by 30% and compared to the control results. Figure 14a shows that a 30% increase ozone across the entire profile lowers and warms the CPT to 16 km (114.1 hPa) with a temperature of 201.2 K. A 30% decrease in ozone raises and cools the CPT to 17 km (96.7 hPa) with a temperature of 200.2 K. Figure 14b shows that a 30% increase causes the LZRH stay at to 14.4 km (150.1 hPa) and the potential temperature at this level decreases

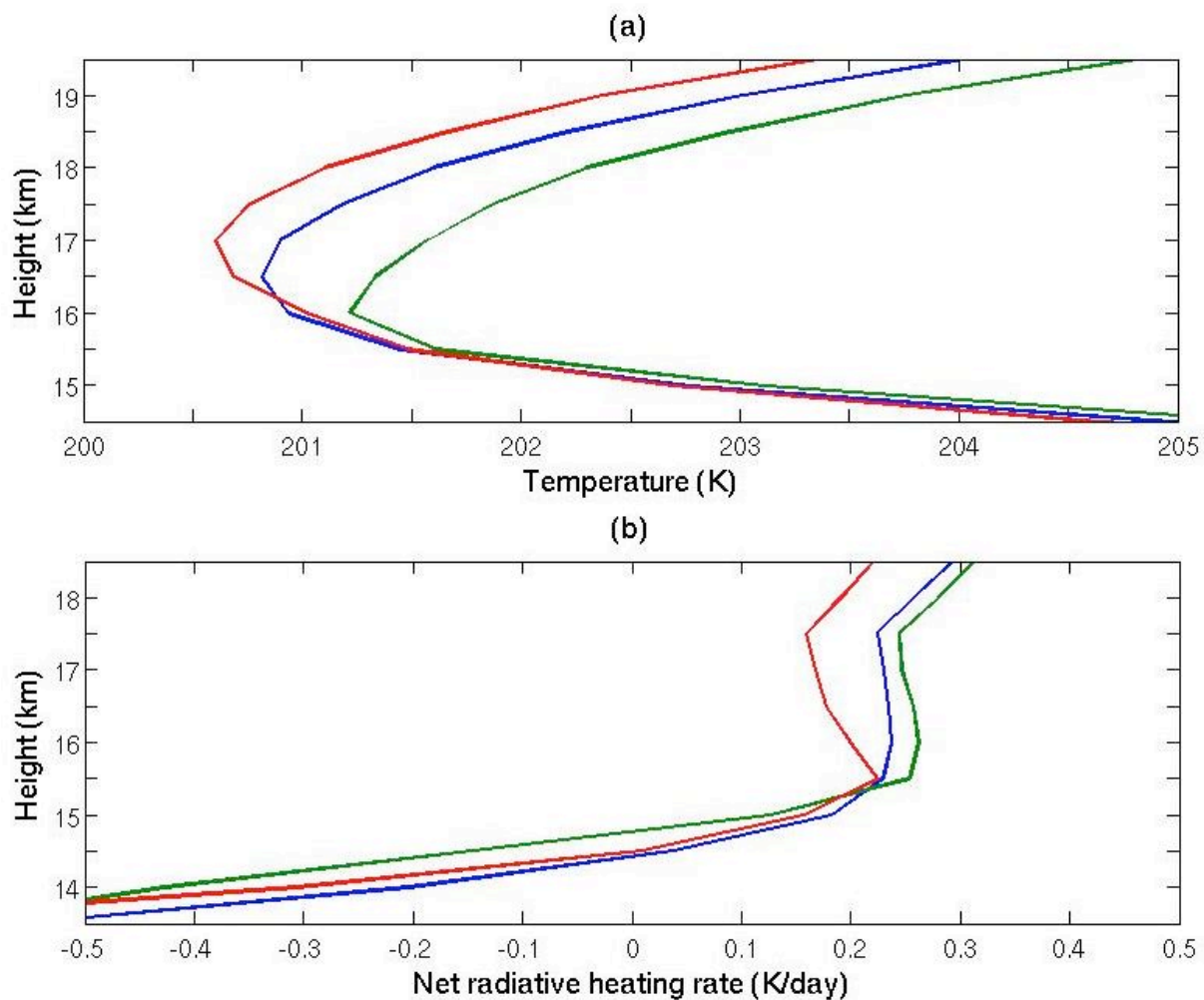


Figure 13: Plot of temperature structure and net radiative heating rate vs. height from the first subset of sensitivity runs where ozone concentration is increased and decreased by 15% over the entire profile. In both a) and b) the green line represents a 15% increase, the red line represents a 15% decrease, and the blue line represents the control run.

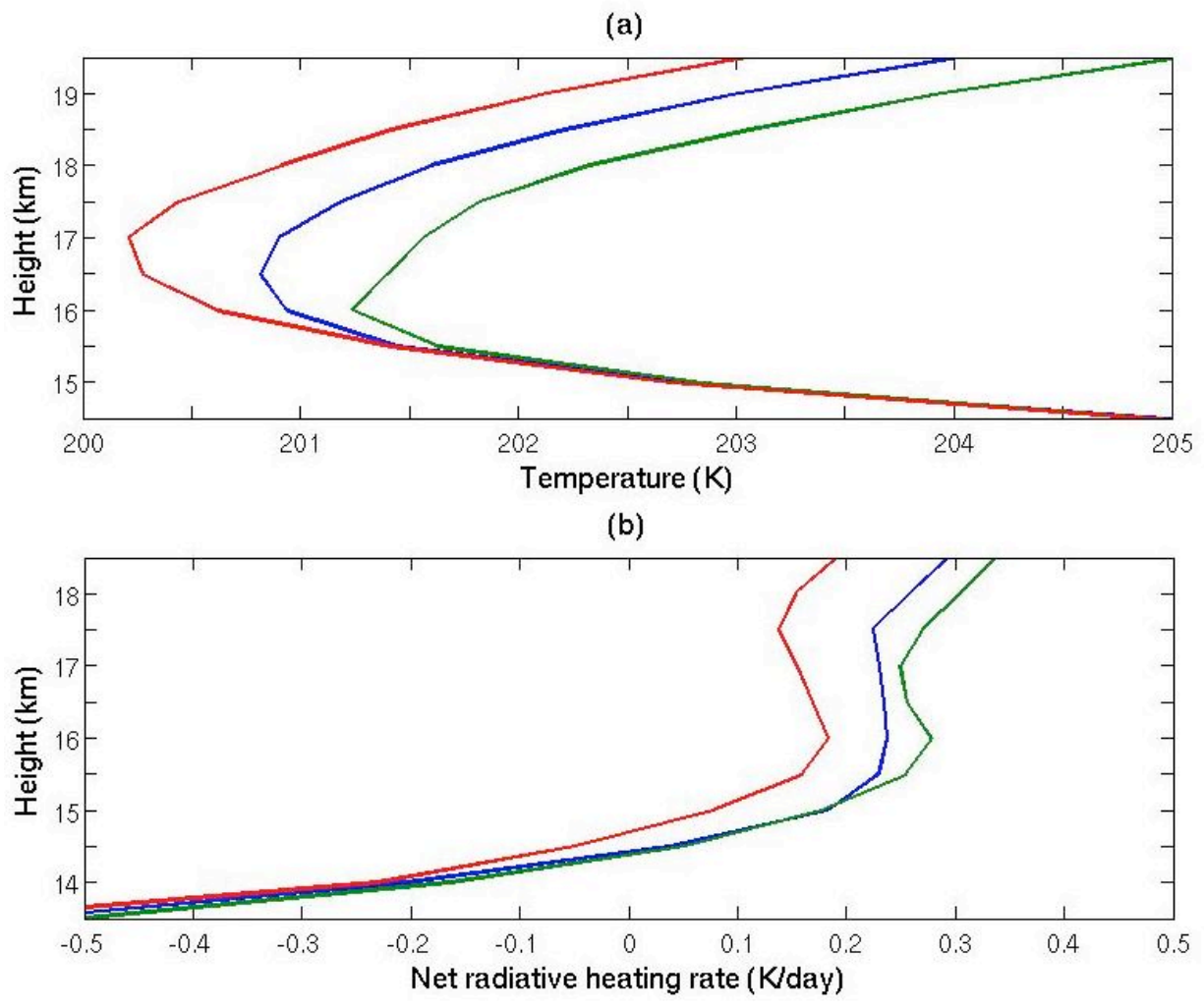


Figure 14: Plot of temperature structure and net radiative heating rate vs. height from the first subset of sensitivity runs where ozone concentration is increased and decreased by 30% over the entire profile. In both a) and b) the green line represents a 30% increase, the red line represents a 30% decrease, and the blue line represents the control run.

very slightly to 353.8 K. A 30% decrease causes the LZRH slightly increases to 14.7 km (143.1 hPa) and the potential temperature increases to 355.8.3 K. The stronger forcing by increasing ozone concentrations does not further increase or decrease the heights of the CPT and LZRH.

5.1.3 O₃ ppmv +/- 15% above 13.5 km

In the third subset of experiments, the ozone concentration was increased and then decreased by 15% above 13.5 km (vertical gradient in ozone) and compared to the control results. Figure 15a shows that a 15% increase ozone above 13.5 km lowers and warms the CPT to 16 km (114.7 hPa) with a temperature of 201.3 K. A 15% decrease raises and cools the CPT to 17 km (96.9 hPa) with a temperature of 200.3 K. Figure 15b shows that a 15% increase causes the LZRH slightly increases to 14.5 km (147.7 hPa) and the potential temperature at this level increases to 354.5 K. A 15% decrease causes the LZRH to rise slightly to 14.6 km (145.7 hPa) and the potential temperature warms to 354.9 K. These results are exceptionally similar to those gathered from the first subset and the second subset where ozone concentration was increased and decreased through the entire profile.

5.1.4 O₃ ppmv +/- 15% below 13.5 km

In the fourth subset of experiments, the ozone concentration was increased and then decreased by 15% below 13.5 km (vertical gradient in ozone) and compared to the control results. Figure 16a shows that a 15% increase ozone below 13.5 km does not change the height of the CPT (16.5 km) and the temperature remains the same at 200.8 K. A 15% decrease does not change the height of the CPT (16.5 km) and the temperature slightly cools

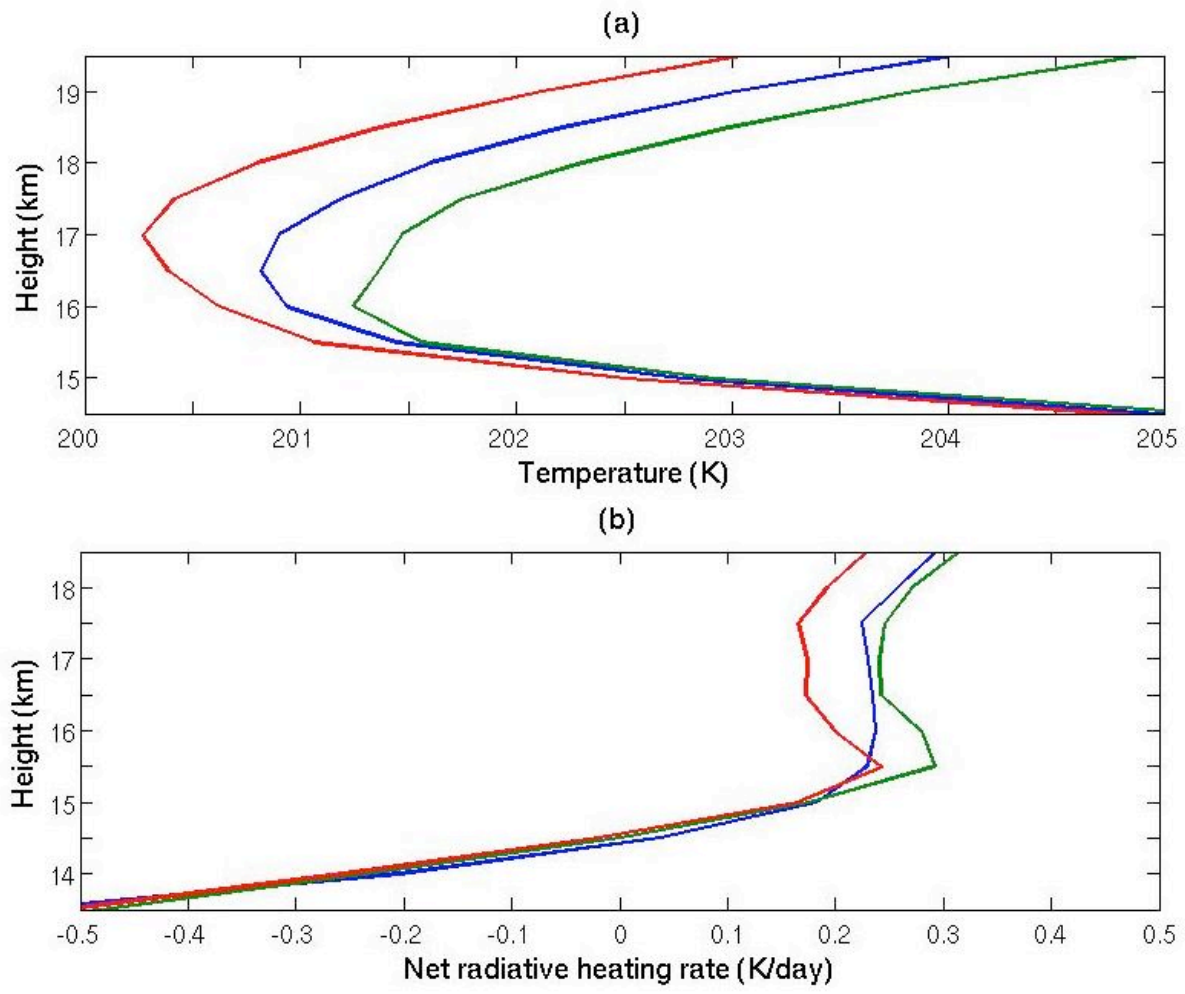


Figure 15: Plot of temperature structure and net radiative heating rate vs. height from the first subset of sensitivity runs where ozone concentration is increased and decreased by 15% above 13.5 km. In both a) and b) the green line represents a 15% increase, the red line represents a 15% decrease, and the blue line represents the control run.

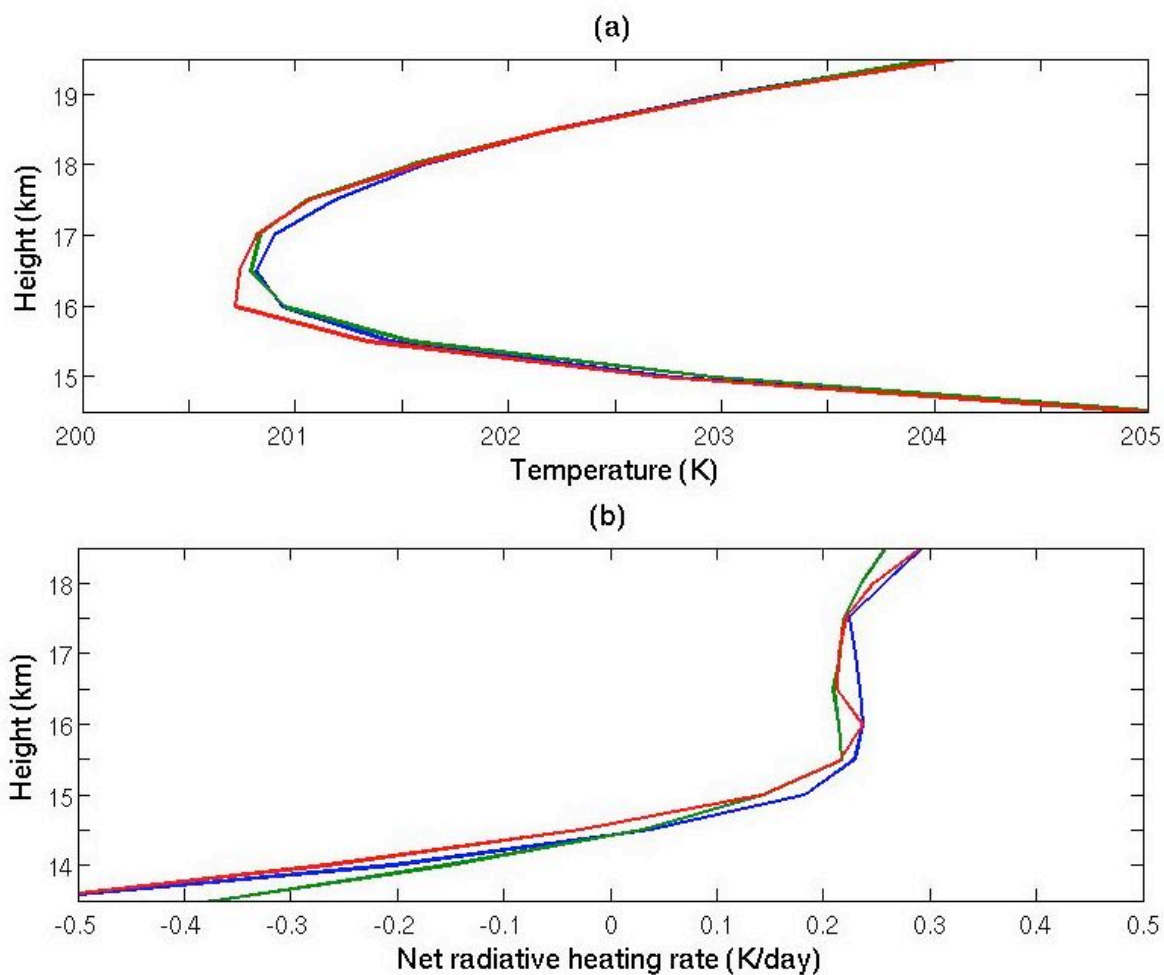


Figure 16: Plot of temperature structure and net radiative heating rate vs. height from the first subset of sensitivity runs where ozone concentration is increased and decreased by 15% below 13.5 km. In both a) and b) the green line represents a 15% increase, the red line represents a 15% decrease, and the blue line represents the control run.

to 200.7 K. Figure 16b shows that with a 15% increase below 13.5 km the LZRH remains at 14.4 km and the potential temperature at this level slightly cools to 357.8 K. While, the LZRH slightly increases to 14.6 km (145.1 hPa) and the potential temperature increases to 355.4 K with a 15% decrease below 13.5 km.

5.2 Summary

Four sets of different sensitivity experiments are conducted in order to test how responsive critical levels in the TTL are to changes in ozone concentration. The temperature and height of the CPT and LZRH are diagnosed in these sets of experiments. In the first two subsets of experiments, when the ozone concentration is increased this causes the CPT to lower and warm, and when the ozone concentration is decreased this causes the CPT to raise and cool. At the CPT ozone warming shifts the equilibrium between ozone warming and water vapor/carbon dioxide cooling towards warmer temperatures and vice versa when concentrations are decreased. An analogous result occurs when ozone profile itself is scaled up or down without changing ozone concentration (e.g. Thuburn and Craig, 2002).

The third and fourth subsets were constructed given the importance of the vertical mixing barrier and its relation to the LMCO. In the third subset where ozone was increased and decreased by 15% above 13.5 km, the results were very similar at the CPT to the increasing or decreasing of the entire profile. Xie et al. (2008) found similar results when conducting an experiment of greenhouse gases using a GCM without the effect of clouds. Qualitatively this makes sense, as above the vertical mixing barrier ozone concentrations grow to over two orders of magnitude larger than concentrations in the lower and middle troposphere. Thus, these higher concentrations will dominate in the context of radiative

equilibrium. In the fourth subset where concentrations were increased and decreased below 13.5 km there was no change felt at the CPT, as expected.

In the first four subsets of experiments the sensitivity of the LZRH was also diagnosed. The LZRH is controlled to a large extent below by longwave cooling as a result to water vapor and above by warming from ozone and carbon dioxide. Therefore, increasing the amount of water vapor around and above the LZRH would cause it to rise, and analogously increasing ozone or carbon dioxide would tend to lower it (e.g. Gettelman et al., 2004). Surprisingly based on the results from this sensitivity study no linear response to increasing or decreasing ozone concentrations to the height or potential temperature can be found. In the four experiments where the ozone concentration was increased, the height of the LZRH stayed the same or increased slightly (up to 0.4 km). In the four experiments where the ozone concentration was decreased the height of the LZRH again stayed the same or increased slightly (up to 0.3 km). The potential temperature at the LZRH fluctuated up to 4 K, but no noteworthy trend could be found. These results contradict those found by Gettelman et al., 2004. They studied radiation processes in the TTL and in particular the LZRH mainly in clear sky cases by using several different models and radiation codes. In cloudy sky cases they did not explicitly simulate deep convection rather they prescribed three different heights and optical thicknesses for these clouds. It is clear here that there must be another mechanism that may be compensating the increased ozone concentration. It seems convection, large scale ascent/descent, and horizontal advection act as a secondary mechanism to modify the LZRH as they can vertically and horizontally modify chemical concentrations of ozone, carbon dioxide, and water vapor. Given that the ozone profiles in

these four subsets of experiments are fixed, potential feedbacks associated with this secondary mechanism are beyond the scope these experiments.

CHAPTER 6

CONCLUSIONS

The tropical tropopause layer, the atmospheric region between the level of main convective outflow and the cold point tropopause, shares properties of the upper troposphere and lower stratosphere. A distinct coupling of dominant convective process occurring in the troposphere and radiatively driven processes occurring in the stratosphere provide the link to the existence of the TTL. Over the past two decades abundant research studies and field campaigns have been conducted with the sole focus of improving understanding of these processes in the TTL. The primary focus of this thesis was to conduct a modeling study of the TTL and the various processes occurring in this region without the need to parameterize the effects of deep convection. A non-hydrostatic cloud resolving model coupled with observational data profiles was used in this study. The goal of modeling was threefold: to fulfill the experiment design to successfully simulate the formation and maintenance of the tropical tropopause layer from an initial tropical sounding including shear, to be able to replicate the types of observations seen during field programs and previous research, and to examine the sensitivity of this layer to various important species and processes within the region.

This CRM study was different than previous studies in that effects of shear were not removed from the initial tropical sounding. Thus, this simulation was a more realistic treatment to gravity waves shed from convection. After inspection of the potential temperature field, there was no evidence found of gravity wave breaking and therefore no

model induced cooling or heating. This design also allowed for the inclusion of longer time scale stratospheric features (e.g. QBO).

The experiment design of the control run fulfilled the first two modeling goals of this study. The control simulation reaches a statistical RCE after ~ 100 days where temperature was still able to fluctuate. The control run successfully simulated the TTL and its critical levels. The LRM was found to be at ~ 10.5 km (275 hPa) and coincident with the LRM was the O_3 min. The LMCO was found to be around the vertical mixing barrier at ~ 13.5 km. The LZRH was located at 14.4 km (150 hPa) and at a potential temperature of 353.9 K. The CPT was found at ~ 16.5 km (105 hPa) at a temperature of 200.8 K. These levels matched well with observational data and previous studies.

Deep convection was explicitly simulated in the control run and it occurred frequently in the control run. There were active and quiet convective periods. Organized tropical squall lines developed lasting on average 8-12 hrs and mean subsidence prevailed in the bulk troposphere outside of convective towers. Most convection detrained at the LMCO around 13-14 km, but there was also evidence of stronger convective updrafts overshooting there LNB into the TTL and above the LZRH. Several deep convective events penetrated above the CPT and into the lower stratosphere where by they were able to directly inject water vapor into the lower stratosphere.

All water vapor above ~ 600 hPa in the averaged tropical sounding was initially removed in order to determine if a combination of deep convection and large scale upwelling could transport enough water vapor into the TTL in the simulation to match observational data and previous studies. The average water vapor concentration in the TTL was around 3.5-

7 ppmv, which is line with observational values from previous studies. Water vapor concentrations of 1.2 ppmv at the CPT were 1.0-1.6 ppmv lower than observational values.

TTL cirrus clouds were present in the TTL region during the control simulation of which most appear to be generated by detrained ice crystals from convective anvils around 13-15 km. These cirrus persisted due to supersaturations with respect to ice and subsequent homogeneous pristine ice crystal formation despite the sedimentation of larger ice particles. There were also TTL cirrus that form in-situ outside of convective events. The simulation was unable to fully resolve the presence of SVC formation (thickness ≤ 500 m) given the vertical resolution and bulk microphysics used.

To test how responsive the TTL was to changes in ozone concentration a series of sensitivity experiments were conducted. Ozone concentrations were increased and decreased by 15% and 30% over the entire tropical ozone profile. When the ozone concentration was increased this caused the CPT to lower and warm, and when the ozone concentration was decreased this caused the CPT to raise and cool. Then, ozone concentrations were increased and decreased by 15% above and below the vertical gradient in ozone (13.5 km). An increase or decrease of ozone above the vertical gradient in ozone cause analogous results to the first two sets of experiments, while increasing and decreasing the ozone concentration below 13.5 km resulted in no appreciable changes to the CPT as expected. The height of the CPT strongly depends on the height at which ozone mixing ratio begins to increase sharply and the temperature of the CPT depends on the balance between ozone heating and water vapor/carbon dioxide cooling.

The height of the LZRH is strongly tied to the balance of longwave cooling by water vapor and warming by ozone and carbon dioxide. Increasing or decreasing the ozone

concentration of the entire profile or above/below the vertical gradient in ozone resulted in each case to increase the LZRH anywhere from 100-300m. It was expected that an increase of ozone concentration would ultimately lower the LZRH by increased radiational warming of ozone as other studies with GCMs or radiation models suggested. Convection or large scale ascent can ultimately change the vertical profile of different chemical species and therefore could provide the necessary feedback by supplying increased amounts of water vapor into the region to counteract the increased ozone concentration.

The last point above introduces the need for further studies in this area. A large amount of attention has been paid to conducting sensitivity experiments of the TTL with the use of static profiles of chemical species such as carbon dioxide, ozone, water vapor, etc in a clear sky radiation models or GCMs without explicitly simulating convection. In the studies where CRMs are used and convection is explicitly simulated, only static profiles such as the ones used in this study are modeled. A logical next step on the basis of this experiment would be to allow the ozone profile to freely advect and partake in radiative processes within the model domain, reach equilibrium with the background vertical motion profile, and then to conduct more a more comprehensive sensitivity study of the TTL based on changes in concentration of the ozone profile. This type of continued study would then allow for the study of the background vertical motion profile and its relation to the changes in the vertical profile of ozone.

Another key point to address in future studies would be incorporating a more complex microphysics package capable of predicting an array of different polycrystals along with hexagonal monocrystals in the UW-NMS CRM. Employing the Advance Microphysics Prediction System (AMPS) including the Spectral Ice Habit Prediction System (SHIPS) (e.g.

Hashino and Tripoli, 2007) would be a logical next step. AMPS would allow for a more complete treatment of microphysical processes occurring in the TTL in particular TTL cirrus formation, maintenance and decay.

REFERENCES

- Adler, R. F., and R. A. Mack, 1986: Thunderstorm cloud top dynamics as inferred from satellite-observations and a cloud top parcel model, *J. Atmos. Sci.*, **43**, 1945-1960.
- Alcala, C. M., and A. E. Dessler, 2002: Observations of deep convection in the tropics using the Tropical Rainfall Measuring Mission (TRMM) precipitation radar, *J. Geophys. Res.*, 107(D24), 4792, doi:10.1029/2002JD002457.
- Baldwin, M. P., and coauthors, 2001: The quasi-biennial oscillation, *Rev. Geophys.*, **39** (2), 179-229.
- Bjerknes, J., 1969: Atmospheric teleconnections from the equatorial pacific. *Mon. Wea. Rev.*, **97**, 163-172
- Brewer, A. W., 1949: Evidence for a world circulation provided by measurements of helium and water vapour distribution in the stratosphere, *Q. J. R. Meteorol. Soc.*, **75**, 351-363.
- Corti, T., B. P. Luo, M. de Reus, D. Brunner, 2008: Unprecedented evidence for deep convection hydrating the tropical stratosphere, *Geophys. Res. Lett.*, **35**, L10810, doi:10.1029/2008GL033641.
- Corti, T., Luo, B. P., Vomel, H., and Peter, T., 2006: The impact of cirrus clouds on tropical troposphere-to-stratosphere transport, *Atmos. Chem. Phys.*, **6**, 2539-2547.
- Corti, T., Luo, B. P., Peter, T., Vomel, H., and Fu, Q., 2005: Mean radiative energy balance and vertical mass fluxes in the equatorial upper troposphere and lower stratosphere, *Geophys. Res. Lett.*, **32**, L06802.
- Danielsen, E., 1993: In situ evidence of rapid, vertical, irreversible transport of lower tropospheric air into the lower tropical stratosphere by convective cloud turrets and by larger-scale upwelling in tropical cyclones, *J. Geophys. Res.*, **98**, 8665-8681.
- Dessler, A. E., S. P. Palm, and J. D. Spinhirne, 2006: Tropical cloud-top height distributions revealed by the ice, cloud, and land elevation satellite (ICESat)/ geoscience laser altimeter system (GLAS), *J. Geophys. Res.*, **111**, D12215, doi: 10.1029/2005JD006705.
- Dessler, A. E., 2002: The effect of deep, tropical convection on the tropical tropopause layer. *J. Geophys. Res.*, **107**, 4033, doi:10.1029/2001JD000511.
- Dinh, T. P., D. R. Durran, and T. P. Ackerman, 2010: Maintenance of tropical tropopause layer cirrus. *J. Geophys. Res.*, **115**, DO2104, doi:10.1029/2009JDO12735.

- Dobson, G. M. B., 1956: Origin and distribution of the polyatomic molecules in the atmosphere, *Proc. R. Soc. London A*, **236**, 187-193.
- Dunkerton, T., 1978: On the mean meridional mass motions of the stratosphere and mesosphere, *J. Atmos. Sci.*, **35**, 2325-2333.
- Durrán, D. R., T. Dinh, M. Ammerman, and T. Ackerman, 2009: The mesoscale dynamics of thin tropical tropopause cirrus. *J. Atmos. Sci.*, **66**, 2859-2873.
- Fierli, F., Di Donfrancesco, G., Cairo, F., Marecal, V., Zampieri, M., Orlandi, E., and Durry, G., 2008: Variability of cirrus clouds in a convective outflow during the Hibiscus campaign, *Atmos. Chem. Phys.*, **8**, 4547-4558.
- Flatau, P., G. J. Tripoli, J. Verlinde, and W. Cotton, 1989: The CSU RAMS cloud microphysics module: General theory and code documentation, Technical Report 451, Colorado State University, 88 pp. [Dept. of Atmos. Sci., Colo. State Univ., Fort Collins, CO, 80523].
- Folkens, I., C. Braun, A. M. Thompson, and J. Witte, 2002: Tropical ozone as an indicator of deep convection, *J. Geophys. Res.*, **107**(D13), 4184, doi:10.1029/2001JD001178.
- Folkens, I., S. J. Oltmans, and A. M. Thompson, 2000: Tropical Convective outflow and near-surface equivalent potential temperatures, *Geophys. Res. Lett.*, **27**(16), 2549-2552.
- Folkens, I., M. Loewenstein, J. Podolske, S. J. Oltmans, and M. Proffitt, 1999: A barrier to vertical mixing at 14 km in the tropics: Evidence from ozonesondes and aircraft measurements, *J. Geophys. Res.*, **104**, 22,095– 22,102.
- Froyd, K. D., Murphy, D. M., Lawson, P., Baumgardner, D., Herman, R. L., 2010: Aerosols that form subvisible cirrus at the tropical tropopause, *Atmos. Chem. Phys.*, **10**, 209-218.
- Fu, Q., Y. Hu, and Q. Yang, 2007: Identifying the top of the tropical tropopause layer from vertical mass flux analysis and CALIPSO lidar cloud observations, *Geophys. Res. Lett.*, **34**, L14813, doi:10.1029/2007GL030099.
- Fueglistaler, S., Dessler, A. E., Dunkerton, T.J., Folkens, I., Fu, Q., and Motes, P.W., 2009: Tropical tropopause layer, *Rev. Geophys.*, **47**, RG1004, doi:1029/2008RG000267.
- Fueglistaler, S., and Q. Fu, 2006: Impact of clouds on radiative heating rates in the tropical lower stratosphere, *J. Geophys. Res.*, **111**, D23202, doi:10.1029/2006JD007273.

- Fueglistaler, S., and Haynes, P. H., 2005: Control of interannual and longer-term variability of stratospheric water vapor, *J. Geophys. Res.*, 110(D24), D24108, doi:10.1029/2005JD006019.
- Garrett, T. J., J. Dean-Day, C. Liu, B. Barnett, G. Mace, D. Baumgardner, C. Webster, T. Bui, W. Read, and P. Minnis, 2006: Convective formation of pileus near the tropopause, *Atmos. Chem. Phys.*, **6**, 1185–1200.
- Garrett, T., A. Heymsfield, M. McGill, B. Ridley, D. Baumgardner, T. Bui, and C. Webster, 2004: Convective generation of cirrus near the tropopause, *J. Geophys. Res.*, **109**, D21203, doi:10.1029/2004JD004952.
- Gettelman, A., Birner, T., Eyring, V., Akiyoshi, H., Bekki, S., Brühl, C., Dameris, M., Kinnison, D. E., Lefevre, F., Lott, F., Mancini, E., Pitari, G., Plummer, D. A., Rozanov, E., Shibata, K., Stenke, A., Struthers, H., and Tian, W., 2009: The Tropical Tropopause Layer 1960–2100, *Atmos. Chem. Phys.*, **9**, 1621–1637, doi:10.5194/acp-9-1621-2009.
- Gettelman, A., D. E. Kinnison, T. J. Dunkerton, and G. P. Brasseur, 2004: Impact of monsoon circulations on the upper troposphere and lower stratosphere, *J. Geophys. Res.*, **109**, D22101, doi:10.1029/2004JD004878.
- Gettelman, A., Forster, P.M.D., Fujiwara, Mu., Fu, Q., Vomel, H., Gohar, L. K., Johanson, C., and Ammerman, M., 2004: Radiation balance of the tropical tropopause layer, *J. Geophys. Res. Atmos.*, **109**, D07 103, doi:10.129/2003JD004190.
- Gettelman, A., and P. M. de Forster, 2002: A climatology of the tropical tropopause layer, *J. Meteorol. Soc. Jpn.*, **80**, 911 – 924.
- Gettelman, A., W. J., Randel, S. Massie, F., Wu, W. G., Read, and J. M., Russell III, 2001: El Niño as a natural experiment for studying the tropical tropopause region, *J. Climate*, **14**, 3375–3392.
- Grabowski, W. W., M. W. Moncrieff, and J. T. Kiehl, 1996a: Long-term behavior of precipitating tropical cloud systems: A numerical study. *Quart. J. Roy. Meteor. Soc.*, **122**, 1019–1042.
- Grosvenor, D. P., Choullarton, T. W., Coe, H., and Held, G., 2007: A study of the effect of overshooting deep convection on the water content of the ttl and lower stratosphere from cloud resolving model simulations, *Atmos. Chem. Phys. Discuss.*, **7**, 7277–7346.
- Hartmann, D. L., Holton, J. R., and Fu, Q., 2001: The heat balance of the tropical tropopause, cirrus, and stratospheric dehydration, *Geophys. Res. Lett.*, **28**, 1969–1972.

- Hashino, T., and G. Tripoli, 2007: The Spectral Ice Habit Prediction System (SHIPS). Part 1: Model description and simulation of vapor deposition process. *J. Atmo. Sci.*, **64**, 2210-2237.
- Haynes, P. H., and E. Shuckburgh, 2000: Effective diffusivity as a diagnostic of atmospheric transport: 2. Troposphere and lower stratosphere, *J. Geophys. Res.*, **105**(D18), 22,795–22,810.
- Held, I. M., and Hou, A. Y., 1980: Nonlinear axially symmetric circulations in a nearly inviscid atmosphere, *J. Atmos. Sci.*, **37**, 515-533.
- Highwood, E. J. and B. J. Hoskins, 1998: The tropical tropopause. *Quart. J. Roy. Meteor. Soc.*, **124**, 1579–1604.
- Holton, J. R., and A. Gettelman, 2001: Horizontal transport and the dehydration of the stratosphere, *Geophys. Res. Lett.*, **28**, 2799–2802.
- Holton, J. R., Haynes, P.H., McIntyre, M. E., Douglass, A.R., Rood, R.B., and Pfister, L., 1995: Stratosphere-troposphere exchange, *Rev. Geophys.*, **33**, 403-439.
- Holton, J. R., 1992: An introduction to dynamic meteorology, 3rd ed. Academic Press, 368-401 pp.
- Immler F., K. Krüger, M. Fujiwara, G. Verver, M. Rex and O. Schrems, 2008: Correlation between equatorial Kelvin waves and the occurrence of extremely thin ice clouds at the tropical tropopause, *Atmos. Chem. Phys.*, **8**, 4019-4026.
- Jacob, D.J., et al., 1996: Origin of ozone and NO_x in the tropical troposphere: A photochemical analysis of aircraft observations over the South Atlantic basin, *J. Geophys. Res.*, **101**, 24235-24520.
- Jensen, E. J., L. Pfister, T.-P. Bui, P. Lawson, and D. Baumgardner, 2010: Ice nucleation and cloud microphysical properties in tropical tropopause layer cirrus. *Atmos. Chem. Phys.*, **10**, 1369-1384.
- Jensen, E. J., Pfister, L., Bui, T. V., Lawson, P., Baker, B., Mo, Q., Baumgardner, D., Weinstock, E. M., et al., 2008: Formation of large (100 μm) ice crystals near the tropical tropopause, *Atmos. Chem. Phys.*, **8**, 1621-1633.
- Jensen, E. J., Ackerman, A. S., and Smith, J. A., 2007: Can overshooting convection dehydrate the tropical tropopause layer?, *J. Geophys. Res.*, **112**, D11209, doi: 10.1029/2006D007943..

- Jensen, E. J., O. B. Toon, L. Pfister, H. B. Selkirk, 1996a: Dehydration of the upper troposphere and lower stratosphere by subvisible cirrus clouds near the tropical tropopause, *J. Geophys. Res. Lett.*, **23**, 825-828.
- Jensen, E. J., O. B. Toon, H. B. Selkirk, J. D. Spinhirne, and M. R. Schoeberl, 1996b: On the formation and persistence of subvisible cirrus clouds near the tropical tropopause. *J. Geophys. Res.*, **101**, doi:10.1029/95JD03575.
- Kazil, J., Lovejoy, E. R., Jensen, E. J., and Hanson, D. R., 2007: Is aerosol formation in cirrus clouds possible?, *Atmos. Chem. Phys.*, **7**, 1407-1413.
- Keeling, R.F., S.C. Piper, A.F. Bollenbacher and J.S. Walker, 2009. Atmospheric CO₂ records from sites in the SIO air sampling network. In Trends: A Compendium of Data on Global Change. Carbon Dioxide Information Analysis Center, Oak Ridge National Laboratory, U.S. Department of Energy, Oak Ridge, Tenn., U.S.A. doi: 10.3334/CDIAC/atg.035,
- Kley, D., J. M. Russell III, and C. Phillips, Eds., 2000: Assessment of upper tropospheric and stratospheric water vapour, *WMO Tech. Doc.*, **1043**, 312 pp.
- Kuang, Z. M., Bretherton C. S., 2004: Convective influence on the heat balance of the tropical tropopause layer: A cloud-resolving model study, *J. Atmos. Sci.*, **23**, 2919-2927.
- Lawson, R. P., Pilon, B., Baker, B. A., Mo, Q., Jensen, E. J., Pfister, L., and Bui, P., 2008: Aircraft measurements of microphysical properties of subvisible cirrus clouds in the tropical tropopause layer, *Atmos. Chem. Phys.*, **8**, 1609–1620.
- Liu, C., and E. J. Zipser, 2005: Global distribution of convection penetrating the tropical tropopause, *J. Geophys. Res.*, **110**, D234, doi: 10.1029/2005JD006063.
- Luo, Z. and W. B. Rossow, 2004: Characterizing tropical cirrus life cycle, evolution, and interaction with upper-tropospheric water vapor using Lagrangian trajectory analysis of satellite observations. *J. Climate*, **17**, 4541–4563.
- McFarquhar, G. M., A. J. Heymsfield, J. Spinhirne, and B. Hart, 2000: Thin and subvisual tropopause tropical cirrus: Observations and radiative impacts. *J. Atmos. Sci.*, **57**, 1841–1853.
- Manabe, S., Wetherald, R. T., 1967: Thermal Equilibrium of the Atmosphere with a Given Distribution of Relative Humidity, *J. Atmos. Sci.*, **24**, 241-259.
- Manabe, S., and R. F. Strickler, 1964: Thermal equilibrium of the atmosphere with convective adjustment, *J. Atmos. Sci.*, **21**, 361–385.

- Massie, S., Gettelman, A., Randel, W., and Baumgardner, D., 2002: Distribution of tropical cirrus in relation to convection, *J. Geophys. Res.*, 107(D21), 4591, doi:10.1029/2001JD001293.
- Mlawer, E.J., and S.A. Clough, 1997b: On the extension of rapid radiative transfer model to the shortwave region, in Proceedings of the 6th Atmospheric Radiation Measurement (ARM) Science Team Meeting, U.S. Department of Energy, CONF-9603149.
- Mlawer, E.J., S.J. Taubman, P.D. Brown, M.J. Iacono and S.A. Clough, 1997a: RRTM, a validated correlated-k model for the longwave. *J. Geophys. Res.*, **102**, 16,663-16,682.
- Mote, P. W., T. J. Dunkerton, M. E. McIntyre, E. A. Ray, P. H. Haynes, and J. M. Russell, 1998: Vertical velocity, vertical diffusion, and dilution by midlatitude air in the tropical lower stratosphere, *J. Geophys. Res.*, **103**, 8651–8666.
- Mote, P. W., and Coauthors, 1996: An atmospheric tape recorder: The imprint of tropical tropopause temperatures on stratospheric water vapor, *J. Geophys. Res.*, 101, 3989-4006.
- Newell, R. E., and S. Gould-Stewart, 1981: A stratospheric fountain? *J. Atmos. Sci.*, **38**, 2789-2796.
- Pfister, L., Selkirk, H. B., Jensen E. J., et al., 2001: Aircraft observations of thin cirrus clouds near the tropical tropopause, *J. Geophys. Res.*, **106** (D9), 9765-9786.
- Peixoto, J.P. and A. H. Oort, 1992: *Physics of Climate*, American Institute of Physics, New York, NY.
- Plumb, R. A., and J. Eluszkiewicz, 1999: The Brewer-Dobson circulation: dynamics of the tropical upwelling, *J. Atmos. Sci.*, **56**, 868– 890.
- Reid, G., and Gage, K., 1985: Interannual variations in the height of the tropical tropopause, *J. Atmos. Sci.*, **38**, 1928-1938.
- Rosenlof, K. H., 1995: Seasonal cycle of the residual mean meridional circulation in the stratosphere, *J. Geophys. Res.*, **100**, 5173-5191.
- Sassen, K. and B. S. Cho, 1992: Subvisual-thin cirrus lidar data set from satellite verification and climatological research. *J. Applied. Meteo.*, **31**, 1275–1285.
- Selkirk, H. C., 1993: The tropopause cold trap during STEP/AMEX 1987, *J. Geophys. Res.*, **98**, 8591-8610.

- Sherwood, S. C., and Dessler, 2001: A model for transport across the tropical tropopause, *J. Atmos. Sci.*, **58**, 765-779.
- Sherwood, S. C., 2000: A stratospheric drain over the maritime continent, *Geophys. Res. Lett.*, **27**, 677– 680.
- Thuburn, J., and G. C. Craig, 2002: On the temperature structure of the tropical substratosphere, *J. Geophys Res.*, 107D, 4017, doi: 10.1029/2001JD000448.
- Tripoli, G. J., 1992: A nonhydrostatic mesoscale model designed to simulate scale interaction, *Mon. Wea. Rev.*, **120**, 1342-1359.
- Wang, P.-H., Minnis, P., McCormick, M., Kent, G., and Skeens, K., 1996: A 6-year climatology of cloud occurrence from stratospheric aerosol and gas experiment II observations (1985-1990), *J. Geophys. Res.*, **101**, 29407-29429.
- Winkler, D. M., and Trepte, C. R., 1998: Laminar cirrus observed near the tropical tropopause by LITE, *Geophys. Res., Lett.*, **25**, 3351-3354.
- Xie, F., Tian, W., and Chipperfield M. P., 2009: Radiative effect of ozone change on stratosphere-troposphere exchange, *J. Geophys. Res.*, **113**, D00B09, doi:10.1029/2008JD009829.
- Zhu, Y., R. E., Newell, and W. G., Read, 2000: Factors Controlling Upper-Troposphere Water Vapor, *J. Climate*, **13**, 836-848.